Engineering Fracture Mechanics 320 (2025) 111086

Contents lists available at ScienceDirect

Engineering Fracture Mechanics

journal homepage: www.elsevier.com/locate/engfracmech

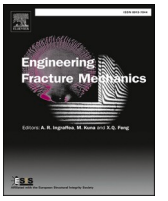

A probabilistic model to consider scale and gradient effects in the prediction of the fatigue life of Inconel 718 for turbine disk application

J.P. Goulmy [a,*], M. Kaminski [b], F.H. Leroy [b], P. Kanoute [b]

[a] Arts et Métiers, Institute of Technology, MSMP, F-13617 Aix-en-Provence, France
[b] DMAS, ONERA, Université Paris-Saclay, 92320 Châtillon, France

ARTICLE INFO

Keywords:
Fatigue
Life prediction
Stress gradient effect
Scale effect
Weibull distribution

ABSTRACT

The aim of this paper is to implement and compare different fatigue post-processing approaches for fatigue life assessment of complex parts. Inconel 718 is taken as an example, as it can exhibit several factors influencing fatigue life, such as mean stress, stress gradient and scale effects. Tests on different specimen geometries to exacerbate these effects were carried out at 550 °C. The range of service operating life is between 10^3 and 10^6 cycles. A modelling chain was then set up. A structural calculation was performed using an elasto-visco-plastic behavior law to obtain the mechanical fields at cycle stabilize. These values were finally exploited by applying a post-processing treatment approach to predict the fatigue life of the structure. Two main types of post-processing approach were investigated: standard and probabilistic. The way in which the different factors influencing fatigue life are considered, depending on the approach used, was discussed. Finally, the probabilistic volume approach yields better results, thanks to its ability to consider mean stress, stress gradient and scale effects in the proposed formulation.

1. Introduction

Fatigue prediction of parts such as turbine disks, blades or airframe assemblies is a major concern for aircraft manufacturers. These parts are subjected to cyclic loads that can lead to crack initiation and part failure. The accurate modelling of the mechanical fields within the part and the estimation of the fatigue behavior are key issues for the safety and mechanical design of the parts. Many factors make it difficult to implement a modelling chain that can predict the fatigue life of complex parts: evolution of the multiaxial mechanical fields in service; effects of mean stress on fatigue life [1,2]; influence of stress gradient on fatigue life [3]; initiation on defect inducing a dispersion of fatigue life and a scale effect [4,5]. Among the parts mentioned above, Inconel 718 turbine disks are particularly sensitive to all of the above factors. Chaboche *et al.* exposed the influence of the mean stress on the fatigue life of Inconel 718 at 550 °C [1]. Chen *et al.* and Amargier have shown that Inconel 718 is sensitive to notch effects, especially at high temperatures [6,7]. Alexandre showed that Inconel 718 was affected by scale effects at 600 °C [8]. The possibility of initiating on inclusions or large grains is one factor generating this scale effect since the initiation is then linked to the probability of finding a preferential initiation site in the material. This effect leads to a strong dispersion of the lifetime data [8,9] on lab specimens tested in fatigue. This phenomenon results in significant variability in the fatigue test lifetime data obtained from laboratory samples. The larger the specimen, the smaller

* Corresponding author.
E-mail address: jean-patrick.goulmy@ensam.eu (J.P. Goulmy).

https://doi.org/10.1016/j.engfracmech.2025.111086
Received 13 January 2025; Received in revised form 4 March 2025; Accepted 26 March 2025
Available online 1 April 2025

Nomenclature

SWT	Smith-Watson-Topper
SCS	smooth cylindrical specimen
DA	Direct Aged
WLS	Weighted Least Squares
FCV	Fracture Characteristic Volume
LCF	Low Cycle Fatigue
HCF	High Cycle Fatigue
VHCF	Very High Cycle Fatigue
M	Weibull modulus
CV	Coefficient of Variation
ML	maximum likelihood
K_f	fatigue stress concentration factor
K_t	elastic stress concentration factor
wt%	weight percentage
R_ε	strain ratio
R_F	load ratio
σ_{max}	maximum local stress
σ_{nom}	nominal stress
$S_{reduced}$	cross-sectional area
F	applied load
LK_t	specimen with $K_t = 1.3$
HK_t	specimen with $K_t = 1.6$
$\boldsymbol{\varepsilon}$	total strain tensor
$\boldsymbol{\varepsilon^e}$	elastic strain tensor
$\boldsymbol{\varepsilon^p}$	plastic strain tensor
$\dot{\boldsymbol{\varepsilon}}^{\boldsymbol{p}}$	plastic strain rate tensor
$\boldsymbol{\Sigma}$	stress tensor
J	von Mises invariant
R	size of the instantaneous yield limit
$\boldsymbol{X}$	back-stress tensor
n, K	Norton parameters
b_i, Q_i	material parameters
C_k, D_k, ω_k	material parameters
σ_{aeff}	effective stress
ε_a	total strain amplitude
σ_a	total stress amplitude
E	Young's modulus
T	ratio of the mean stress to the stress amplitude
ε_{aeq}	equivalent strain amplitude
σ_{aeq}	equivalent stress amplitude
t_{eq}	ratio of the mean value of the stress tensor trace to the equivalent amplitude of the stress
$(Tr\sigma)_{mean}$	mean value of the stress tensor trace
b, b'	material parameters
A and α	material parameters
N_f	number of cycles as failure
R90C95	distribution with a reliability of R = 90 and a confidence level of C = 95 %, Owen model
R50C50	regression model of Basquin identified with Weigthed Least Squares
V	volume of the specimen
S	surface of the specimen
$\Omega_r(\boldsymbol{x})$	domain of radius r centered on $\boldsymbol{x}$
$\Omega^*(\boldsymbol{x})$	effective volume of material in the domain $\Omega_r(\boldsymbol{x})$
r_c	radius length
μ	scaling factor
C,β	material parameters
P_s^i	survival probability of the finite element i for a number of cycles less than N
$P_s(N)$	survival probability of the structural model
n_e	number of finite elements in the model

V_e^i	volume of element i
S_e^i	surface area of the element i
V_g^i	volume assigned to each Gauss point

the dispersion. Therefore, they provide a particularly interesting case study for discussing the implementation of different fatigue life modelling strategies. In addition, the presence of stress concentrations in the structure induces depth stress gradients and stress confinement in the concentration zone. The part is therefore sensitive to several factors simultaneously: mean stress, stress gradient, and scale effects. Taking this into account is a major challenge in the design of fatigue structures.

Most fatigue lifetime models are expressed in cycles with phenomenological formulations relating σ, ε, or energy, to the number of cycles to initiation [1]. Another possibility is the use of coupled approaches where a damage variable is associated with an evolution law, also written in terms of the number of cycles [10,11]. More recently, incremental models have been developed where the evolution law of the damage variable depends on time [12,13].

One advantage in using phenomenological formulations is the opportunity to introduce easily the effects of mean stress. So, extensions of the Manson Coffin criterion such as Walker, Morrow, or SWT can be considered [14]. Among these extensions, the SWT model has already been successfully used by Chaboche *et al.* to translate the impact of the mean stress on the fatigue life of Inconel 718 at 550 °C [1]. Because of their geometry, turbine disks have a complex mechanical field that can induce multiaxiality effects that need to be considered. Several multiaxial criteria can be found in the literature. These criteria are classified into three main categories. A constraint invariant approach leads to the use of criteria such as those of Sines, Crossland, or Gonçalvès [15,16,17]. A second approach concerns energy models [18]. Finally, the generalization of this type of criterion in multiaxial can be accomplished using the concept of a critical plane, as shown by the models of Brown and Miller, Fatemi and Socie, and Robert [19,20,21]. As a result, there are many formulations, but no real consensus on the accuracy of one over the other to estimate shear and equibiaxial fatigue conditions together with mean-stress effects. In this context Bonnand *et al.* proposed a new multiaxial criterion that generalizes the SWT model, and has been applied with a good accuracy to several multiaxial test conditions [22].

Gradient effects represent the fact that service life is not driven solely by the maximum value present in the part, but is also a function of the gradient of the driving force (stress, *etc.*) for crack initiation surrounding this point. For some materials, such as Inconel 718, this factor is far from negligible. Different methods have been suggested since the 1940 s to improve the consideration of these effects. The oldest ones involve calculating the fatigue stress concentration factor K_f from the elastic stress concentration factor K_t [23,24]. They have the advantage of being relatively simple but prove inadequate when dealing with different sample geometries. These concentration factors may be identical even if the experimental fatigue limits differ. Many criteria based on non-local approaches have been developed to more accurately assess the influence of stress gradients on fatigue life. Among them, we can mention methods using the notion of critical distance developed by Neuber and Peterson [23,24]. They have been successfully applied to a wide range of materials, including single crystal material, following an elasto-visco-plastic calculation to evaluate the mechanical fields in the vicinity of notches or holes [13]. These approaches are based on a standard deterministic lifetime assessment, which does not allow consideration of the scale effects. To our knowledge, only a few papers have developed methodologies that combine a standard deterministic approach with the consideration of scale effects [4,25]. These methods can therefore be particularly interesting, but require the use of numerous specimens of different geometries to be implemented.

Scale or size effects represent the fact that the fatigue life of a part depends on the volume it is subjected to. This notion is closely linked to the probability of finding a defect of a certain size in a volume. The larger the volume under load, the greater the probability of finding the defect. Scale effects are often concomitant with gradient effects. The gradient effect could be considered as the simply influence of the non-uniform distribution of the driving force extended over the volume, area or length investigated, on the probability of failure due to the scale effect.

To consider size or scale effects, it is thus often necessary to apply a probabilistic model. Two methods are used in the literature: the direct approach and the indirect approach. The direct approach consists of modelling the randomness at its source by using a characterization of the defects present in the material. The quantity most consistently associated with scattering at initiation and discussed in the literature is then the endurance limit. Probabilistic scaling approaches focus essentially on this quantity with "weakest link" type models, a weibullian distribution of the endurance limit is then estimated [26,27]. This direct approach was also investigated by Alexandre to predict the fatigue life of smooth cylindrical specimens of Inconel 718 DA at 600 °C, where surface and internal initiation had been observed [8]. In contrast to direct approaches, there are indirect approaches for which only measurements of lifetimes and loading estimates are available. Although limiting, this type of approach is relatively common and, in particular, allows for the description of a lifetime regime ranging from 10^3 to 10^6 cycles. For these methods, the probabilization is based on the logarithm of the fatigue life of the volume (or surface) element [28]. The main hypothesis is based on a Gaussian distribution of the evolution of the logarithm of the number of cycles, associated with a Basquin power law evolution of the average lifetime. However, this law is not well adapted to the consideration of scale effects. In this case, it is preferable to assume a Weibullian evolution for the evolution of the logarithm of the number of cycles [29,30], as did Karolczuk *et al.* [31].

Although many models exist in the literature to assess the fatigue life of Inconel 718 [1,9,32,33], they present specificities that do not allow all the constraints mentioned above to be considered. The aim of this paper is to implement and compare different fatigue post-processing approaches for assess fatigue life assessment of Inconel 718 parts that may include scale and gradient effects, such as turbine disks.

The paper is divided into three sections. Section 2 is dedicated to the presentation of the experimental results. The material and the

Table 1
Composition of the Inconel 718 DA Alloy (Wt%).

Ni	Fe	Cr	Mo	Al	Ti	Nb	Si	C
54.18	17.31	17.97	2.97	0.56	1	5.39	0.1	0.023

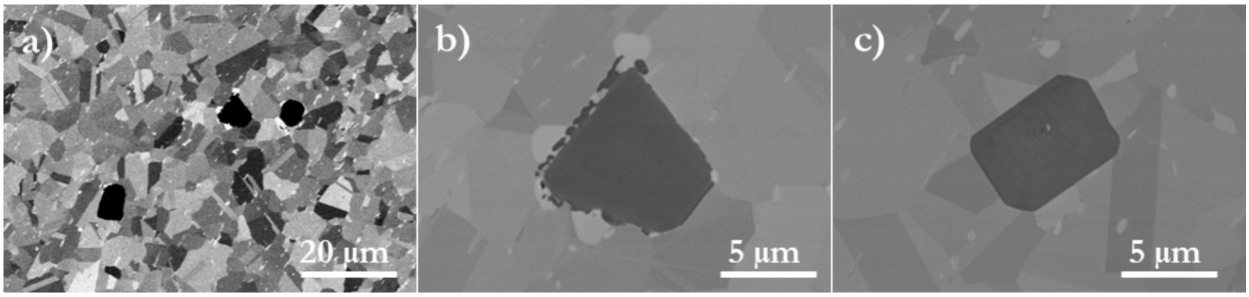

Fig. 1. Scanning electron microscopy observations of Inconel 718 DA a) grains; b) titanium and niobium carbide; c) titanium nitride.

test conditions are introduced. Inconel 718 smooth and notch specimens are characterized by fatigue loading at 550°C. The fatigue results are discussed for the different geometries, and the fatigue fractography analyzes are given. The fatigue life prediction scheme is presented in Section 3. The different post-processing approaches are introduced and the parameters of the different approaches are identified from the data obtained for smooth specimens. The modelling chain is then applied to the case of stress concentration specimens in Section 4. Finally, the different post-processing approaches are compared regarding the experimental data.

2. Experimental results

2.1. Material and experimental procedure

The investigated material is Inconel 718 Direct Aged (Table 1). It should be noted that the material used in this study is identical to that referenced in [1,34], which are cited throughout this document (for all batches), including the same composition and grain size. Furthermore, the stress–strain curves for both tensile and cyclic behavior can also be found within these references. The characterization of the microstructure has been carried out by scanning electron microscopy observations (Fig. 1) and backscatter electron analyses. A mean grain size of 5 µm was observed with maximum values of 20 µm. The analyzed samples also contain a significant number of nitrides and carbides ranging from 5 to 10 µm in size.

More than thirty fatigue tests were carried out on two different samples: smooth cylindrical samples (with a diameter of 4 mm and an effective length of 60 mm) and notched cylindrical samples (dimensions detailed below). The smooth cylindrical specimens (SCS) were used to assess the cyclic behavior of the material and to determine the fatigue life of specimens subjected to uniaxial loading. Experimental tests were carried out under conditions simulating a typical turbine disc environment (temperature of 550 °C). Using an MTS hydraulic testing machine equipped with a 10 kN load cell, varying load ratios (R_ε) of 0, 0.6 and −1 were applied. The tests were strain controlled using an extensometer with a working length of 25 mm. The strain rate applied was 10^{-3} s^{-1}. Testing was stopped when specimen failure was observed. The corresponding fatigue data are respectively named Batch1, Batch2 and Batch3 in the following. In addition, for comparison, the results obtained from previous test campaign on the same material and under similar conditions (strain controlled tests) have also been added (Batch Chaboche *et al.*, $R_\varepsilon = 0$) [1].

Notch specimens were used to evaluate the influence of a notch on the fatigue lifetime. Recall that the stress concentration coefficient is defined as the ratio of the maximum local stress (calculated in elasticity) σ_{max} to the nominal stress σ_{nom}, that would be present on a fictitious specimen in which the notch has been removed and reduced to its cross-sectional area $S_{reduced}$.

$$\mathbf{K_t} = \frac{\sigma_{\mathbf{max}}}{\sigma_{\mathbf{nom}}} \mathbf{with} \sigma_{\mathbf{nom}} = \frac{\mathbf{F}}{\mathbf{S_{reduced}}} \tag{1}$$

To evaluate how the mechanical field near the notch affects the fatigue life of Inconel 718, two stress concentrations were investigated: $K_t = 1.3$ and $K_t = 1.6$ named LK_t and HK_t specimens in the following. These values were selected to represent the stress concentrations encountered on turbine disks. Since the specimens have different dimensions, particular attention was paid to identify the scale effects apart from the gradient effects. The tests on notch specimens were also performed at 550 °C on the same hydraulic fatigue device. The experiments were conducted at a frequency of 10 Hz and a load ratio of $R_F = 0$. The levels of strain and stress applied to the gauge section of the notched specimens (see Fig. 5) remained under the material's yield strength. Consequently, the regulation of strain and stress seems to be quite comparable. Regardless, monitoring the test at the base of the notch was impractical. Utilizing stress control allowed for a higher frequency of testing, which led to reduced test durations compared to those conducted under strain control.

Following testing, mid-life data (stress amplitude, mean stress) were determined, and fatigue fracture analyses were performed

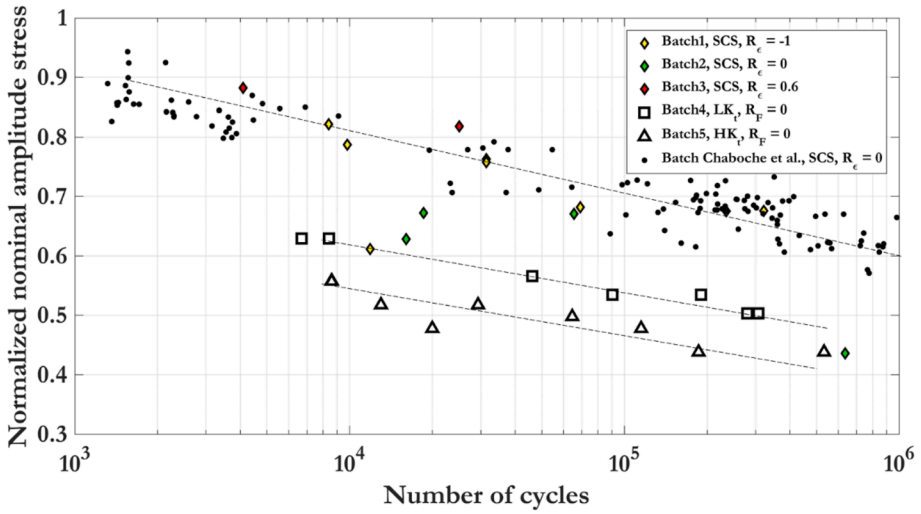

Fig. 2. Fatigue life of Inconel 718 for different specimen geometries at 550 °C. Experimental data and data extract from [1].

using a scanning electron microscope. Note that in the following, all data are normalized.

It has been demonstrated in the literature that loading rates can affect the fatigue life of materials, generally increasing fatigue life with higher frequencies [35]. The higher the temperature and the greater the load, the more significant the impact. Conversely, no impact on fatigue life is observed when the regime is purely elastic. In the present case, tests on smooth specimens induce strain rates of the order of 10^{-3} s^{-1}, while tests on notched specimens induce strain rates of less than 10^{-1} s^{-1}. Additionally, Inconel 718 was loaded at 550 °C with a target life interval of 10^3 to 10^6 cycles. Thus, the effect of loading rates remains moderate. Furthermore, the behavior law used is of the elasto-visco-plastic type (see section 3.1), which can be used to predict the effect of a change in strain rate on stress.

2.2. Fatigue testing

Fatigue data is now compared. Fig. 2 shows the normalized nominal amplitude stress as a function of the number of cycles. The curve normalization (for nominal amplitude stress) was carried out for confidential reasons following an approach similar to [1]. Trends are highlighted with dotted lines. As expected, for a fixed amplitude of nominal stress, an increase in K_t value induces a decrease in fatigue lifetime. For tests on HK_t specimens (Batch5), a decrease in fatigue life by a factor of two to three decades can be observed compared to smooth specimens. The LK_t specimens (Batch4), which present a more limited gradient of the stress field (see section 3.3.2), have a longer life but are still one to two decades shorter than the smooth specimens. As the tests on smooth specimens were carried out at imposed strain, cyclic stress relaxation occurred [1]. Therefore, the values shown here represent mid-life data, when it is generally accepted that stress stabilization has been achieved. For the smooth specimens, there is a noticeable scatter of the data, but a clear trend remains. For the Onera data (Batch1, 2 and 3) the fatigue life is reduced for $R_\varepsilon = 0$ and $R_\varepsilon = 0.6$ with positive mean stress values in comparison to the fully reversed data ($R_\varepsilon = -1$). As discussed by Chaboche [1], the fatigue life regime examined here results in limited mean stress relaxation (less 20 MPa), resulting in positive mean stress values when compared to the fully reversed test condition (experimentally observed to be close to zero as expected). Moreover, a positive mean stress has a negative effect on fatigue life by reducing fatigue strength, as has been widely discussed in the literature.

2.3. Fatigue fractography morphology

Fractography on smooth specimens revealed several key points. The initiation could be surface or subsurface (at 20 μm from the surface). A statistical study on 170 specimens showed that 5 % of the initiations occurred in the subsurface (Batch1, Batch2 and Batch3 and Batch Chaboche *et al.*). Then, the initiation could take place on an inclusion or on a grain. Fig. 3.a shows an example of surface initiation, while Fig. 3.b displays subsurface initiation on a smooth specimen. An Energy Dispersive X-Ray Spectroscopy analysis confirmed that the initiation site shown in Fig. 3.b was a titanium niobium nitride with a size of close to 20 μm. This inclusion was surrounded by grains that were much smaller than the inclusion size. Connolley et *al.* showed that the oxidation generated at 600 °C during the fatigue test on Inconel 718 plays a crucial role in the initiation mechanisms. It leads to an increase in the carbide's size and nitride particles over time, which induces a local stress concentration on the surface of the specimen and thus favors surface initiation [36]. The size of the inclusions observed, in this work, after initiation also confirms these observations at 550 °C. Indeed, the inclusions responsible for the initiation were two to three times larger than those characterized on an unstressed specimen (between 5 and 10 μm (see Fig. 1.b and Fig. 1.c)). Because the observed microstructures are homogeneous in grain size [37], initiation preferentially occurs on inclusions, particularly those whose size is larger than the size of the surrounding grains, is favored (Fig. 3.b). Similar analyzes were conducted on the notch specimens (Fig. 3.c and Fig. 3.d). The results are very close to the smooth specimens. The initiation was the

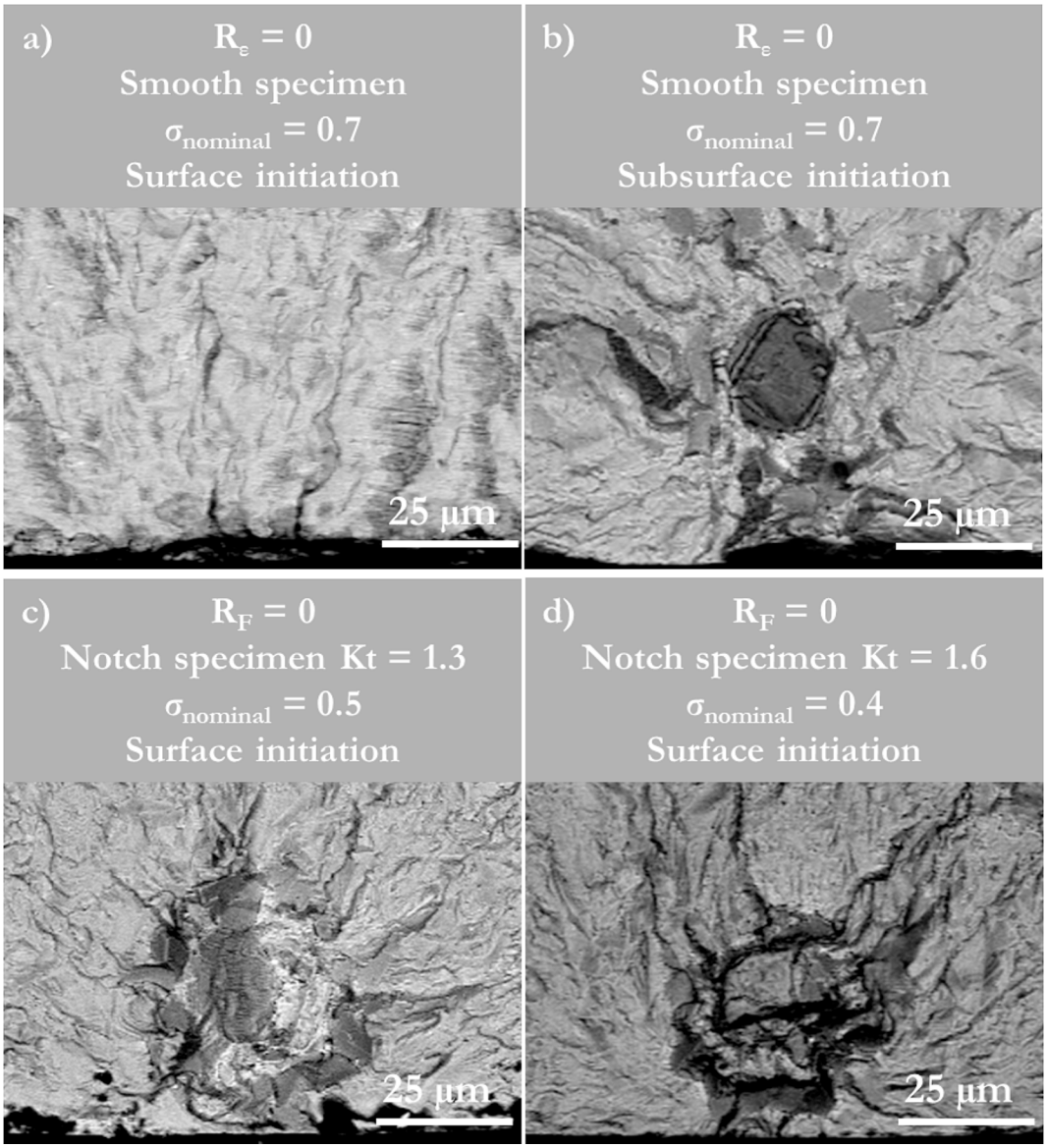

Fig. 3. Examples of fractographies observed on the specimens: a) and b) smooth specimens with surface and subsurface initiation respectively, c) LK_t specimen ($K_t = 1.3$), and d) HK_t specimen ($K_t = 1.6$).

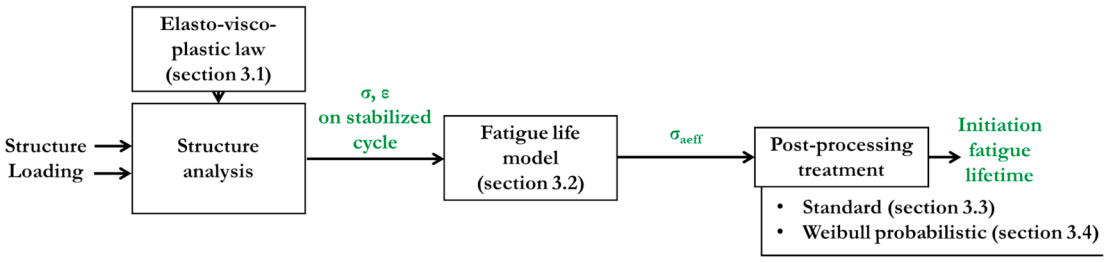

Fig. 4. Scheme of calculation of fatigue life initiation.

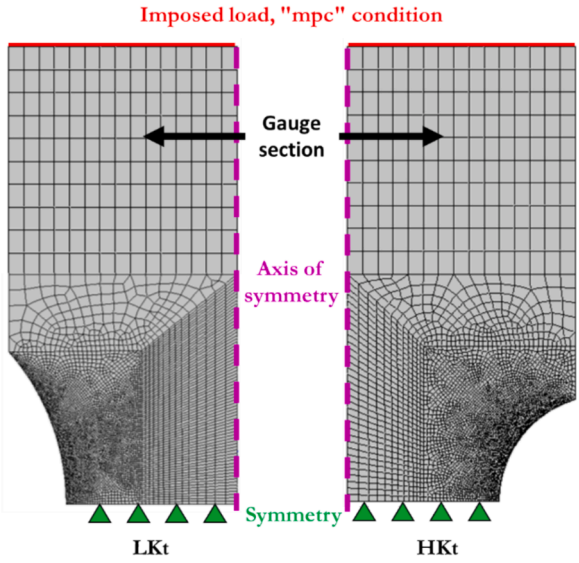

Fig. 5. Meshing and application of boundary conditions to notch specimens.

same for both notch values and for the different loading levels applied. It occurred on the surface, on a grain, on an inclusion or a niobium heterogeneity that has a size greater than 20 μm. This value does not incorporate the initial stage I phase of crack propagation, which corresponds to the regime of short cracks before reaching a stable crack growth regime described by Paris's law. What we will refer to as initiation in subsequent discussions corresponds to the onset of stage II crack propagation.

3. Fatigue life assessment methodology

A post-processing approach was used to predict the fatigue life of Inconel 718 specimens (Fig. 4). This approach is classically used for the fatigue life assessment metallic structures [38]. It consists of three steps:

(i) A structural calculation was performed using an elasto-visco-plastic behavior law [1]. Cycling loading conditions were applied to the structure until a stabilized cycle was obtained.
(ii) The mechanical fields obtained at the stabilized cycle were then used as input to the fatigue model. This model allows the determination of the effective stress at any point of the part.
(iii) A post-processing treatment was then applied to estimate the fatigue life of the structure. Based on the literature review and experimental results, two types of approaches were investigated: standard deterministic (named standard in the following) and probabilistic.

a) The standard approach has been used in the past to estimate the fatigue life of Inconel 718 DA with success on smooth specimens [1]. The fatigue damage model was calibrated to provide an average fatigue life. The observed scatter data was then not considered. It is nevertheless possible to define conservative evaluation using a statistic analysis of the scatter data based on the approximate Owen tolerance limit [39]. The application of such methodology to our fatigue data will be presented later. In addition, few studies have evaluated the ability of the standard approach to estimate the fatigue life of complex structures where both gradient and scale effects are occurring. To account for stress gradients, it has been widely noted in the literature that at least a non-local type of approach is required. In this work, it is proposed to consider gradient effects using the critical distance approach [40,41].
b) On the other hand, the use of a probabilistic approach could allow for partial or full consideration of gradient and scaling effects, depending on whether the surface or the volume of the parts is considered [42]. Typically, the application on the surface could be justified by the surface initiation observed for the different specimen designs (see section 2.3), whereas treatment in the volume may be more relevant in the presence of a stress gradient for a notch specimen.

Note that all the material parameters in the fatigue evaluation chain have been identified using smooth specimens only, as the present chain is independent of the structure used. In contrast to smooth fatigue specimens, where the stress field is uniform throughout the gauge length, specimens with stress concentration have non-uniform stress fields that need to be estimated by finite element analysis. All the specimens were then modelled using the Zset software suite co-developed by Onera and Mines Paris Tech [43]. Symmetry conditions were applied to the central edge and bottom of the specimens as shown in the Fig. 5. A load was applied to the specimen and a multi-Point Constraint condition was used to ensure uniform displacement of all nodes as in the test. The mesh used was axisymmetric and was refined to account for the stress gradient induced in the notch specimen. An analysis of the number of cycles required to stabilize the mechanical fields was carried out to ensure that a number of 1000 cycles was sufficient to reach the stabilized

cycle.

3.1. Elasto-visco-plastic law

The chosen constitutive model to evaluate the mechanical field on stabilized cycle was an elasto-visco-plastic law proposed by Chaboche *et al.* [1]. In this model, the total strain tensor $\boldsymbol{\varepsilon}$ is additively decomposed into the elastic ε^{e} and plastic ε^{p} strain tensors. The elastic domain is defined by $f \leq 0$ in the stress space $\boldsymbol{\sigma}$ with:

$$\mathbf{f} = \mathbf{J}(\sigma - \mathrm{X}) - \mathbf{R} \tag{2}$$

where the function J returns the von Mises invariant, R is the size of the instantaneous yield limit and $\boldsymbol{X}$ is the back-stress tensor. The plastic strain rate tensor $\dot{\boldsymbol{\varepsilon}}^{\boldsymbol{p}}$ is obtained with the flow rule, using the normality assumption:

$$\dot{\varepsilon}^{\mathrm{p}} = \dot{\lambda}\frac{\partial \mathbf{f}}{\partial \sigma} \tag{3}$$

where the dot represents the differentiation regarding time and the plastic multiplier $\dot{\lambda}$ is given by the Norton power law:

$$\dot{\lambda} = \left\langle \frac{\mathbf{f}}{\mathbf{K}} \right\rangle^{\mathbf{n}} \tag{4}$$

To model visco-plasticity, the equivalent plastic strain rate $\dot{p}$ is:

$$\dot{\mathbf{p}} = \sqrt{\frac{2}{3}\dot{\varepsilon}^{\mathrm{p}} : \dot{\varepsilon}^{\mathrm{p}}} \tag{5}$$

A non-linear isotropic hardening R is defined as the sum of several contributions indexed by "*i*":

$$\mathbf{R} = \sum_{\mathbf{i}} \mathbf{R}^{\mathbf{i}} \mathbf{with} \dot{\mathbf{R}}^{\mathbf{i}} = \mathbf{b_i}\left(\mathbf{Q_i} - \mathbf{R}^{\mathbf{i}}\right)\dot{\mathbf{p}} \tag{6}$$

where the b_i and Q_i are material parameters associated to contribution *i*. Similarly, the back stress $\boldsymbol{X}$ is decomposed as the sum of several contributions, indexed with "*k*":

$$\mathrm{X} = \sum_{\mathbf{k}} \mathrm{X}^{\mathbf{k}} \tag{7}$$

with:

$$\dot{\mathrm{X}}^{\mathrm{k}} = \frac{2}{3}\mathbf{C_k}\dot{\varepsilon}^{\mathrm{p}} - \mathbf{D_k}\psi\left(\mathrm{X}^{\mathbf{k}}\right)\mathrm{X}^{\mathbf{k}}\dot{\mathbf{p}} \tag{8}$$

And where the $\psi\left(\boldsymbol{X}^{k}\right)$ is:

$$\psi\left(\mathrm{X}^{\mathbf{k}}\right) = \left\langle \frac{\mathbf{D_k}\mathbf{J}\left(\mathrm{X}^{\mathbf{k}}\right) - \omega_{\mathbf{k}}\mathbf{C_k}}{1 - \omega_{\mathbf{k}}} \right\rangle \frac{1}{\mathbf{D_k}\mathbf{J}\left(\mathrm{X}^{\mathbf{k}}\right)} \tag{9}$$

where C_k, D_k and ω_k are material parameters associated to each contribution *k*. Note that the functions $\psi\left(\boldsymbol{X}^{k}\right)$ contain a threshold effect.

This behavior law allows the cyclic softening characteristic of Inconel 718 at 550 °C to be reproduced as well as the partial relaxation of the mean stress over the fatigue cycles. The ability of the model to describe this effect is particularly important because of the significant effect of the mean stress on the fatigue life of Inconel 718. The material parameters have been rigorously validated through comprehensive comparisons between experimental data and simulations, encompassing monotonic and cyclic behavior, as well as mean stress relaxation as a function of the applied strain in fatigue tests. These comparisons are illustrated in Chaboche et al. [1]. Thus parameters used in this work are identical to those used in [1].

3.2. Fatigue life model

The fatigue life model used in this paper is derived from the classical Manson Coffin model which is based on the partitioning of the total strain amplitude into elastic strain amplitude and plastic strain amplitude. It has been observed that many metallic materials, such as Inconel 718 are sensitive to the effects of mean stress on fatigue life. Therefore, a simple Manson Coffin law is not suitable to account for these effects. Extensions of the Manson-coffin criterion such as Walker, Goodman, or SWT have been then proposed to overcome such limitations [14]. Among these models, the SWT model has already been successfully used by Chaboche *et al.* to investigate the effects of the mean stress on the fatigue life of Inconel 718 at 550 °C [1]. The effective stress introduced by Smith-Watson-Topper is then rewritten as:

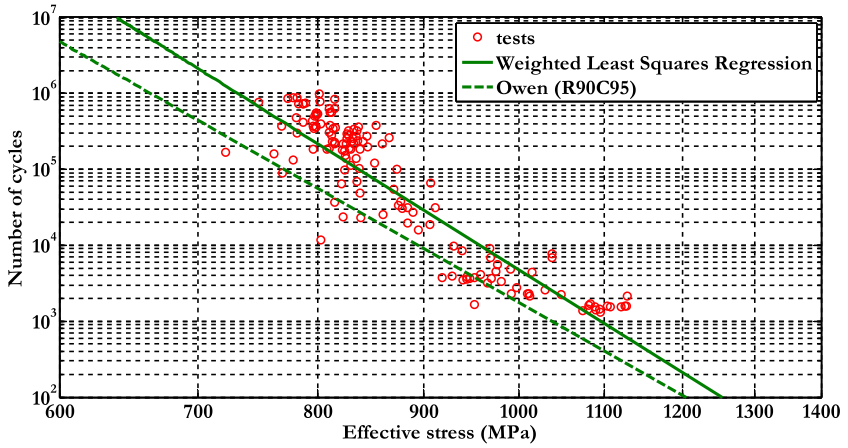

Fig. 6. Weighted least squares regression technique applied on experimental data.

$$\sigma_{\mathbf{aeff}} = \sqrt{\mathbf{E}\varepsilon_{\mathbf{a}}\sigma_{\mathbf{a}}}\mathbf{f}(\mathbf{t}) \tag{10}$$

where ε_a and σ_a are the total strain and stress amplitude, respectively, and E is the Young's modulus of the material. t is the ratio of the mean stress to the stress amplitude (σ_{mean}/σ_a). The effective stress amplitude σ_{aeff} is then a key variable that considers the influence of multiple dependent quantities $\{\varepsilon_a, R_\varepsilon, \sigma_a, R_\sigma, \sigma_{mean}\}$ on the fatigue life.

Due to their geometry, notch specimens have a complex mechanical field at the bottom of the notch (location of fatigue crack initiation) which can induce multiaxiality effects that need to be considered. Based on Bonnand *et al.* work [22], Eq. (10) can be generalized and becomes:

$$\sigma_{\mathbf{aeff}} = \sqrt{\mathbf{E}\varepsilon_{\mathbf{aeq}}\sigma_{\mathbf{aeq}}}\mathbf{f}(\mathbf{t}_{\mathbf{eq}}) \tag{11}$$

where σ_{aeq} represents the equivalent stress amplitude, ε_{aeq} is the equivalent strain amplitude, and t_{eq} is the ratio of the mean value of the stress tensor trace to the equivalent amplitude of the stress (Eq. (12). Remember that the values presented here represent those obtained at the stabilized cycle. Thus, two assumptions are made: (i) the number of cycles required to reach stabilization (i.e., where the mechanical fields no longer evolve) is significantly lower than the number of cycles preceding crack initiation, and (ii) changes in the effective stress during the initial stabilization cycles have a negligible impact on both the underlying damage mechanisms and the subsequently estimated fatigue life.

For proportional loading, the equivalent stress amplitude corresponds to the von Mises of the eigen stress amplitude. For more complex loading conditions, a specific calculation is required, which is described in detail in [44].

$$\mathbf{t}_{\mathbf{eq}} = \frac{(\mathbf{Tr}\sigma)_{\mathbf{mean}}}{\sigma_{\mathbf{aeq}}} \tag{12}$$

From the Haigh diagram, a break in the stress evolution amplitude can be observed for the studied material at a lifetime of 10^5, 10^6 or 10^7 cycles [1]. To reproduce this trend, the function $f(t_{eq})$ is then defined as follows:

$$\mathbf{f}(\mathbf{t}_{\mathbf{eq}}) = \begin{cases} 1 + b.\mathbf{t}_{\mathbf{eq}} si \mathbf{t}_{\mathbf{eq}} < \mathbf{t}_{\mathbf{eq}}^{*} \\ 1 + (\mathbf{b} - \mathbf{b}').\mathbf{t}_{\mathbf{eq}}^{*} + \mathbf{b}'.\mathbf{t}_{\mathbf{eq}} si \mathbf{t}_{\mathbf{eq}} > \mathbf{t}_{\mathbf{eq}}^{*} \end{cases} \tag{13}$$

where b and b' are the values of the slopes and t_{eq}^{*} represents the value for which the intersection of the two slopes is observed. Note that the function $f(t_{eq})$ is modified when the mean stress is less than 0 and is written:

$$\mathbf{f}(\mathbf{t}_{\mathbf{eq}}) = (1 - \mathbf{t}_{\mathbf{eq}})^{-1} \tag{14}$$

The material parameters b, b', and t_{eq} are the same as those used in [1] as they have already been determined on a large set of stress ratios using stress-controlled tests.

Finally, the relationship between the effective stress defined in Equation (11) and the number of cycles to crack initiation is expressed as follows:

$$\sigma_{\mathbf{aeff}} = \mathbf{A}\mathbf{N}_{\mathbf{f}}^{-\alpha} \tag{15}$$

where A and α, are material parameters that need to be identified. The sections below outline the procedure for determining these parameters, depending on whether a standard or probabilistic approach was used.

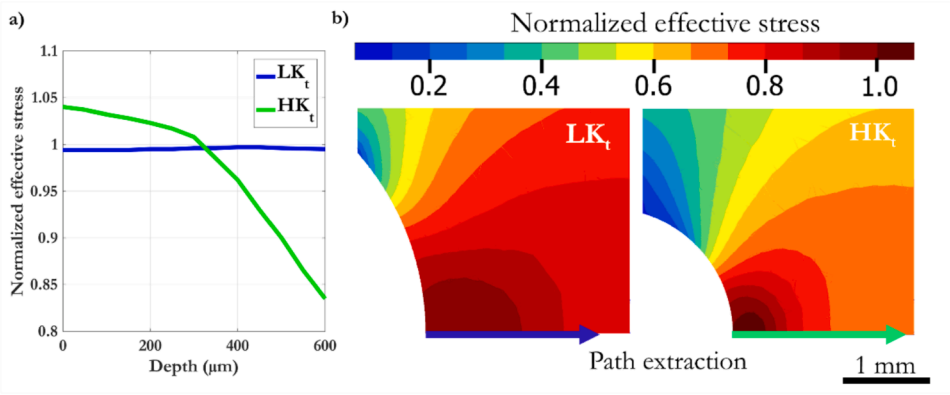

Fig. 7. Example of effective stress gradient observed in the thickness of notch specimens.

3.3. Standard fatigue estimation procedure

3.3.1. Standard methodology

In this section, we demonstrate the application of the approach typically implemented in an industrial context. Our goal is not to merely note the conservatism that has already been highlighted in some cases reported in the literature. Instead, we aim to explain why these methods may be inadequate by illustrating the case of predicting the service life of Inconel 718.

In engineering, simple *S-N* curves are usually plotted by linearly regressing the log*(N)* against log*(S)* data (which corresponds to a Basquin model) and determining a mean *S-N* curve with the standard deviation. A normal log distribution of the number of cycles to failure is generally assumed. Safety margins are then established by applying a correction with standard deviations of 2σ and 3σ to the mean curve, resulting in safety factors over the entire fatigue range. The design curve can be derived by shifting the median stress–life curve in logarithmic coordinates to the left by two or three times the sample standard deviation. This procedure is recommended in particular by the standard [45]. A weighted least squares regression technique was applied to the available data (Fig. 6). N_f was chosen as dependent variable because N_f is clearly affected by a high degree of dispersion which is why we consider the adjustment of the $N_f(\sigma_{aeff})$. The identified regression coefficients for the Basquin law are $A = 1599.9$ MPa and $\alpha = 0.0553$. The corresponding regression is plotted with the green line in Fig. 6.

A statistical analysis has also been conducted using a method based on the approximate Owen tolerance limit. Our database shows that the scatter of logarithmic fatigue life log*(N)* increases as the effective stress level σ_{aeff} decreases. This is called heteroscedasticity. The application of Owen's approach to heteroscedastic life data was not possible in its original form. Sudret *et al.* [46] have proposed a method for considering heteroscedasticity in linear regression. The maximum likelihood method has been adapted for the case of a constant coefficient of variation (standard deviation proportional to the mean). The authors present a description of life expectancy but unfortunately do not provide a quantile estimate with a confidence specification. Therefore, it was necessary to adapt Owen's approach to this heteroscedastic context and more specifically to the assumption of constancy of the coefficient of variation. This has been done in this work within the framework of Weighted Least Squares (WLS) illustrated in Fig. 6 with the dotted green line. The use of the weighted Owen approach allowed for the estimation of a conservative distribution R90C95 with a reliability of R = 90 and a confidence level of C = 95 %. The corresponding identified regression coefficients for the Basquin law are: $A_{R90C95} = 1623$ MPa and $\alpha_{R90C95} = 0.0647$.

3.3.2. Standard methodology with stress gradient effect

As explained in the introduction, Inconel 718 is sensitive to notch effects, especially at high temperatures [2,3].

In this study, K_t specimens were used to be representative of industrial parts. This provides a stress gradient at the bottom of the notch. To ensure this, elasto-visco-plastic calculations were carried out on both specimen geometries. The results, shown Fig. 7, indicate the obtained normalized effective stresses for applied loadings of 0.63 and 0.44 in nominal stress for LK_t and HK_t specimens respectively. For these loadings, the LK_t specimen has a relatively small effective stress gradient in depth. At the same time, the variation in effective stress in the first three hundred microns is of the order of 8 % for the HK_t sample. Due to plastification at the bottom of the notch, which reduces the stress induced by the notch, the stress gradient is more important above three hundred microns (Fig. 7.a).

Unfortunately, the standard approaches described in paragraph 3.3.1 do not allow gradient effects to be taken into consideration. Other methods must therefore be implemented. Among the approaches that consider gradient effects a non-local one seems to be the most effective: the Fracture Characteristic Volume (FCV), applied eventually after an elasto-visco-plastic calculation [47]. Therefore, it was decided to apply it here. The principle of the method is to calculate the fatigue lifetime based on averaged mechanical quantities. Before the post-processing, the stress field is integrated on a representative volume V of the material of radius r (sphere in 3D, circle in 2D) such that:

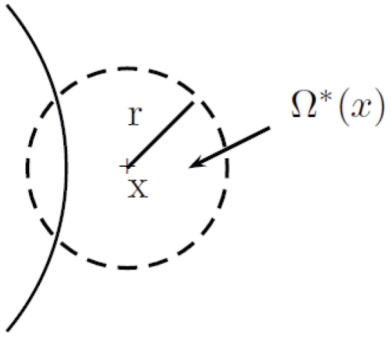

Fig. 8. Representation of the domain $\Omega_r(x)$ of radius r centered at x.

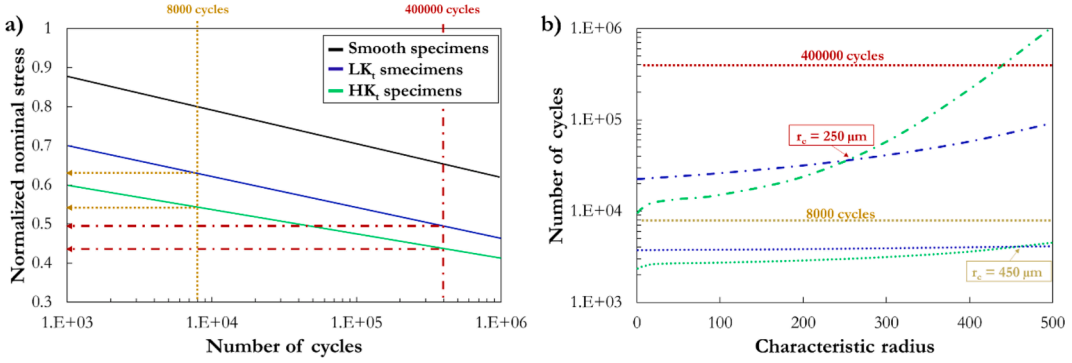

Fig. 9. Identification of a characteristic radius to account for gradient effect.

$$\langle\sigma(\mathbf{r})\rangle = \frac{1}{\mathbf{V}}\int_{\mathbf{V}} \sigma \mathbf{dV} \tag{16}$$

The average is only calculated for the part of the material located in the solid, so the exact formulation of the average is given by:

$$\langle\sigma(\mathbf{x})\rangle = \frac{1}{\Omega^*(\mathbf{x})}\int_{\Omega_r(\mathbf{x})} \sigma(\mathbf{y})\mathbf{dy} \tag{17}$$

where $\Omega_r(x)$ is the domain of radius r centered on x and $\Omega^*(x)$ represents the effective volume of material in the domain $\Omega_r(x)$ (Fig. 8):

$$\Omega^*(\mathbf{x}) = \int_{\Omega_r(\mathbf{x})} \mathbf{dy} \tag{18}$$

The radius length r_c, considered in the modelling is expected to be relative to the predicted crack size and independent of the geometry of the specimen. However, it depends on the material and temperature.

The methodology for determining the characteristic radius r_c is as follows. The nominal stresses required to achieve an identical experimental fatigue life (using the fatigue life model described in 3.2) were determined from tests conducted on stress concentration specimens and smooth specimens (Fig. 9.a). To simplify the approach, a linear relationship between lifetime and the nominal stress was assumed in a logarithmic diagram. Two lifetimes were selected for this approach, 8000 cycles and 400,000 cycles. The normalized nominal stress values for reaching 8000 cycles were 0.63 and 0.55 for LK_t and HK_t specimens respectively. For 400,000 cycles, the normalized nominal stress values applied were 0.49 and 0.45 for LK_t and HK_t specimens respectively. These loads were applied to both specimen geometries and an elasto-visco-plastic calculation was carried out. Based on the mechanical fields obtained at the stabilized cycle, the FCV approach was applied by varying the values of the possible characteristic radius. Note that in this work the effective stress defined in 3.2 has been averaged as this quantity corresponds to the driving force in the chosen fatigue model.

Next, the predicted number of initiation cycles was plotted as a function of the characteristic radius used to carry out the post-processing (Fig. 9.b). The characteristic radius r_c should then correspond to the intersection of the curves showing the number of cycles as a function of the integration radius. Consequently, if there is a notch effect and only a notch effect, then it is assumed that there is a characteristic radius r_c which allows the target lifetime to be obtained for the two geometries tested.

For the target lifetime of 8000 cycles, the intersection of the two curves occurs at a characteristic radius of 450 µm and the predicted lifetime is 4000 cycles. For the target lifetime of 400,000 cycles, the two curves intersect at a characteristic radius of 250 µm, giving an estimated lifetime of 35,000 cycles. Apart from the fact that the service life obtained is lower than expected (this is discussed in more

detail in section 4), the determined characteristic radius is dependent on the level of applied stress, which does not respect the fundamental assumption of FCV approach. In view of the results obtained, the gradient effect does not appear to be the only factor to be consider in the modelling. So, it seems that other approaches need to be implemented. Nevertheless, it was decided to use the two characteristic radii identified here to predict fatigue life with this model for comparison with the experimental data set covering a large range of fatigue life. The results are discussed in section 4.

3.4. A Weibull probabilistic approach

The standard approach described in the previous paragraphs may be sufficient when initiation occurs on grains. However, in the presence of particles crack initiation, as is the case for Inconel 718, this approach may not be sufficient to predict fatigue life correctly. In addition to the gradient effects induced by the shape of the specimens, scale effects can have a major impact on fatigue life due to the change in stressed volume, which varies from one specimen to another [48]. In the case of Inconel 718, the scale effect is favored by the probability of fatigue initiation on particles other than grains (carbides or nitrides). These particles are identical in size or larger than the average grain size. It is therefore natural that fatigue crack initiation is favored by the presence of these particles in the stressed zone. As a result, the lifetime of the part is directly linked to their presence. Based on this observation, Alexandre used a so-called direct probabilistic approach to predict the fatigue life of Inconel 718 DA at 600 °C, where surface and internal initiation were observed [32]. He assessed the impact of the size of the stressed surfaces by characterizing different geometries of smooth specimens (with surface of 1 mm^2, 10 mm^2, and 100 mm^2). The orders of magnitude of the surfaces characterized can be considered similar to the surfaces stressed during this study for HK_t, LK_t and smooth specimens, respectively. He showed that the smaller the surface area representative of the stressed zone, the lower the probability of finding a particle greater than a given critical particle. Highly stressed volumes or surfaces become smaller as the stress concentration of the specimens increases (Fig. 7). Thus, the probability of initiating on a carbide or nitride is influenced by both the size and the shape of the specimens. Based on the work of Alexandre, the probability of finding a particle larger than 30 μm is zero for the HK_t specimen, around 5 % for the LK_t specimen and 50 % for the smooth specimen. As a result, the specimen with the lowest probability of finding a particle larger than a given size has a longer lifetime. Based on these observations, a probabilistic approach of the "weakest link" type was implemented in this study. Because it is necessary to have a large number of specimens of different dimensions to identify the parameters of direct approaches, an indirect approach was proposed in the following.

3.4.1. Description and identification of model parameters

The primary objective here is not to predict the endurance limit but to have a probabilistic description of the Low Cycle Fatigue (LCF) and High Cycle Fatigue (HCF) regimes. For indirect approaches, the choice of probabilization is based on the log-life of the volume (or surface) element. The majority assumption, followed by [49], is that of a Gaussian distribution for *logN* (log-normal distribution) associated with an evolution of $\overline{logN}$ in power law of the stress (or effective stress in our case) (Basquin's law). A dispersion of the log-life proportional to its mean is generally observed and this is accounted for by an additional parameterization of the Coefficient of Variation (*CV*). The objective of probabilistic scale change pursued here leads to prefer the Weibull hypothesis ([29,30]), which is better adapted to this context (as is also the case in [31]). This choice of the log-Weibull hypothesis is based on several arguments.

The first argument is specific to the material studied in this paper (Inconel 718 DA at 550 °C). A preliminary study was conducted on the dispersion of log-life at an imposed strain amplitude (this study was not developed further here). This study indicated an asymmetry in favor of Weibull's law. However, the sample sizes considered are still too small to reject hypothesis of normality using a statistical test. The aforementioned is generally observed in published fatigue studies, where uncertainty persists due to the insufficiency of the statistical tests. This is often due to the limited amount of experimental data available. In this case, it is also advisable to choose the log-Weibull distribution whose asymmetry and thickness of the tails are more penalizing (a conservative choice). Finally, it worth noting that some historical fatigue studies favor the log-Weibull option since fatigue lifetime is driven by extreme value distribution [50].

The second argument is that the log-Weibull distribution law is particularly useful for studying structural lifetime because it simplifies the change of probabilistic scale through numerical integration, as detailed in section 3.4.2.

For the chosen hypothesis, the probability of observing a log-life less than or equal to *logN* is expressed as follows:

$$\mathbf{P}(\boldsymbol{log}(\mathbf{N})) = 1 - \boldsymbol{exp}\left(-\frac{1}{\mathbf{V_o}} \iiint_{\mathbf{V}} \left(\frac{\mathbf{log}(\mathbf{N})}{\boldsymbol{\mu}(\sigma)} \right)^{\mathbf{m}} \mathbf{dV} \right) \tag{19}$$

where m is the Weibull modulus (or shape factor). The modulus m governs the relative lifetime dispersion, which is the ratio of the standard deviation of the distribution to its mean. This is also known as the Coefficient of Variation (*CV*). μ is the characteristic log-life (or scaling factor). μ is close to the mean life $\overline{logN}$ with a maximum difference of 10 % for $m \in [1,20]$. The probability of having $logN < \mu$ is independent of m and is $P(\mu) = 1\text{-}e^{-1} = 0.632$.

It can also be seen that the increase in log-life for Inconel 718 DA is associated with an increase in dispersion in the same proportion ($CV = cst$). This is consistent with observations made in the literature [49]. This can be easily accounted for in Weibull law by introducing the influence of loading at the level of the characteristic log-life.

This study specifically focuses on the domain of finite life, whereas industry typically addresses the domain of infinite endurance through a separate approach. This involves defining a fatigue threshold using maximum likelihood estimation for a service life set at 10^7 cycles. To assess the severity of various loading conditions, they rely on the use of a multiaxial Haigh diagram to analyze the potential impact of load trajectories. Alternative methodologies within a probabilistic framework are available in existing research for

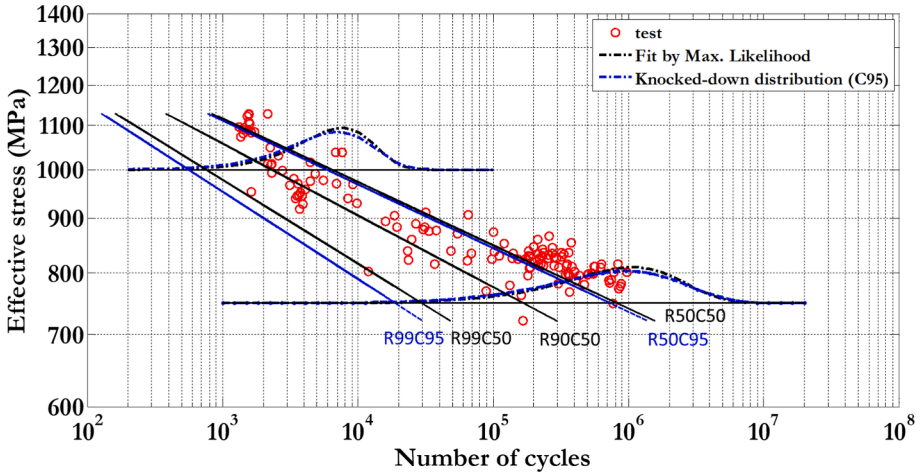

Fig. 10. Accelerated Log-Weibull identification on Inconel 718 DA at 550 °C for a load ratio $R_\varepsilon = 0$. The parameters are specified in Table 2.

Table 2
Identified coefficients of accelerated log-Weibull model: fitting with maximum likelihood (in black in Fig. 10) and knocked-down distribution (in blue in Fig. 10).

	Fitting with maximum likelihood	Knocked-down distribution (95 % confidence)	
C	1681.4 MPa	$C^{95\%}$	1677 MPa
β	0.0579	$\beta^{95\%}$	0.058
m	15.16	$m^{95\%}$	13.41
CV	8.10 %	CV	9.10 %

integrating High Cycle Fatigue (HCF) and Very High Cycle Fatigue (VHCF) domains [51].

Choosing a multiaxial fatigue criterion and applying the classical Basquin hypothesis for both the LCF and HCF domains (power law), we obtain:

$$\sigma_{\mathbf{aeff}} \approx \mathbf{C}\mathbf{N}^{-\beta} \rightarrow \boldsymbol{\mu} = -\frac{1}{\beta}\boldsymbol{log}\sigma_{\mathbf{aeff}} + \frac{1}{\beta}\boldsymbol{log}\mathbf{C} \tag{20}$$

The characteristic log-life therefore shows a linear development in a $logN - \log \sigma_{aeff}$ diagram. It has a constant relationship with $\overline{logN}$ which also depends on m:

$$\overline{\mathbf{logN}} = \boldsymbol{\mu}\Gamma\left(1 + \frac{1}{\mathbf{m}}\right) \tag{21}$$

With:

$$\Gamma\left(1 + \frac{1}{\mathbf{m}}\right) = \frac{1}{\mathbf{m}}! \tag{22}$$

The choice of $\mu \approx f(\sigma_{aeff})$ and m constant corresponds to what is known as an accelerated life cycle model [52]. The dispersion increases with μ and thus with $\overline{logN}$:

$$\mathbf{std}(\mathbf{logN}) = \boldsymbol{\mu}\sqrt{\Gamma\left(1 + \frac{2}{\mathbf{m}}\right) - \Gamma^2\left(1 + \frac{1}{\mathbf{m}}\right)} \tag{23}$$

Note that some authors also introduce a variation of the Weibull m modulus with loading ([31]) in order to include the low cycle fatigue regime.

Finally, it is essential to note that μ is also associated with the volume V_0 or the surface S_0 of the specimens that present defect populations in relation to their scale and that will be used for the identification:

$$\boldsymbol{\mu} = \mathbf{f}\left(\sigma_{\mathbf{aeff}}, \mathbf{V}_0\mathbf{or}\mathbf{S}_0\right) \tag{24}$$

In the present work, the effective stress is uniform in the gauge length of the specimens used for the identification process. When considering specimens with stress field heterogeneity, it is then necessary to introduce the stress heterogeneity factor, which defines the effect of the loading pattern on the cumulative failure probability. From a probabilistic perspective, it describes the fact that a flaw

is critical if it is large enough in a significantly loaded zone [53].

As far as we know, there is currently no standard identification method available for the probabilistic model defined by Eq.20 and Eq.21. Although the relationship is linear, a standard least squares regression tool cannot account for the Weibullian character of the dispersion and the evolution of its amplitude. Therefore, we have chosen to implement the maximum likelihood (*ML*) identification method, which is a central approach in statistics. This method draws on the work of Prudente *et al.* [54]. It is detailed in Appendix A. The quantiles of the probabilistic model have also been used to define a conservative lifetime law. Identification may be subjected to random error due to the limited number of measurements available. It is important to consider this statistical uncertainty when conservative characteristics are desired, such as R99 laws. These laws must be corrected to account for their identification uncertainty. The notion of confidence was used. The methodology is explained in Appendix B. Finally, the identification of the accelerated Weibull model is illustrated in Fig. 10. Corresponding parameters are listed in Table 2.

3.4.2. Prediction of structural lifetime

In the following, the lifetime of the structure is predicted using a "weakest link" approach based on the probabilistic description of the lifetime of each link/finite element *i*. This approach avoids the need for a costly Monte-Carlo type of simulation where the lifetime of each finite element would be drawn at random according to its load and volume and the weakest one would be determined. This process would have to be repeated a large number of times to determine a probability distribution, a conservative law, *etc.*

The survival probability of the finite element *i* for a number of cycles less than *N* is denoted P_s^i. Assuming the independence of the mechanisms leading to the failure of each element (separation of the scales), the survival probability of the structural model $P_s(N)$ can be expressed as follows:

$$\mathbf{P_s}(\mathbf{N}) = \prod_{\mathbf{i}=1}^{\mathbf{n_e}} \mathbf{P_s^i}(\mathbf{N}) \tag{25}$$

where n_e is the number of finite elements in the model.

If we write:

$$\mathbf{P_s^i}(\mathbf{N}) = \mathbf{e}^{-\mathbf{f^i(N)}} \Longrightarrow \mathbf{P_s}(\mathbf{N}) = \boldsymbol{exp}\left(-\sum_{\mathbf{i}=1}^{\mathbf{n_e}} \mathbf{f^i}(\mathbf{N}) \right) \tag{26}$$

The chosen Accelerated Weibull law for the lifetime corresponds to an exponential form which results in this type of simplification. By making this choice:

$$\mathbf{f^i}(\boldsymbol{ln}(\boldsymbol{N})) = \frac{\mathbf{V_e^i}}{\mathbf{V_o}} \left(\frac{\boldsymbol{ln}(\mathbf{N})}{\boldsymbol{\mu}(\sigma^i)} \right)^{\mathbf{m}} \tag{27}$$

V_e^i denotes the volume of element *i*, V_0 is the volume of the fatigue specimens for which the relationship $\mu(\sigma)$ has been identified and σ^i is the equivalent stress experienced by element *i* which is assumed to be uniform per element. Note, that we can also use S_0, the surface of the fatigue specimens and S_e^i the surface area of the element when surface

approach is chosen.

Then we have:

$$\mathbf{P_s}(\boldsymbol{ln}(\mathbf{N})) = \boldsymbol{exp}\left(-\frac{1}{\mathbf{V_o}} \iiint_{\mathbf{V}} \left(\frac{\mathbf{ln}(\mathbf{N})}{\boldsymbol{\mu}(\sigma)} \right)^{\mathbf{m}} \mathbf{dV} \right) \tag{28}$$

By explicitly introducing Basquin's law to describe the loading dependence of the characteristic lifetime $\mu(\sigma)$:

$$\mathbf{P}(\boldsymbol{ln}(\mathbf{N})) = 1 - \boldsymbol{exp}\left(-\frac{1}{\mathbf{V_0}} \iiint_{\mathbf{V}} \left(\frac{\mathbf{ln}(\mathbf{N})}{\frac{1}{\beta}\mathbf{ln}\left(\frac{\mathbf{C}}{\sigma}\right)} \right)^{\mathbf{m}} \mathbf{dV} \right) \tag{29}$$

After rearrangement, and considering the parameters identified for the conservative estimate at 95 % confidence, we obtain the result:

$$\begin{cases} P(\boldsymbol{ln}(\mathbf{N})) = 1 - \boldsymbol{exp}\left(-\left(\dfrac{\mathbf{ln}(\mathbf{N})}{\boldsymbol{\mu}_{\mathbf{struct}}} \right)^{\mathbf{m^{95\%}}} \right) \\ \boldsymbol{\mu}_{\mathbf{struct}} = \dfrac{1}{\beta^{95\%}} \left(\dfrac{\mathbf{I}}{\mathbf{V_0}} \right)^{-\frac{1}{\mathbf{m^{95\%}}}}, avecI = \iiint_{\mathbf{V}} \boldsymbol{ln}\left(\dfrac{\mathbf{C^{95\%}}}{\sigma} \right)^{-\mathbf{m^{95\%}}} \mathbf{dV} \end{cases} \tag{30}$$

Firstly, the overall structural life also follows a Weibull distribution with the same modulus *m* as a uniformly fatigued specimen. Additionally, a lower lifetime limit (R99C95) can also be determined relative to the average lifetime, without any post-processing:

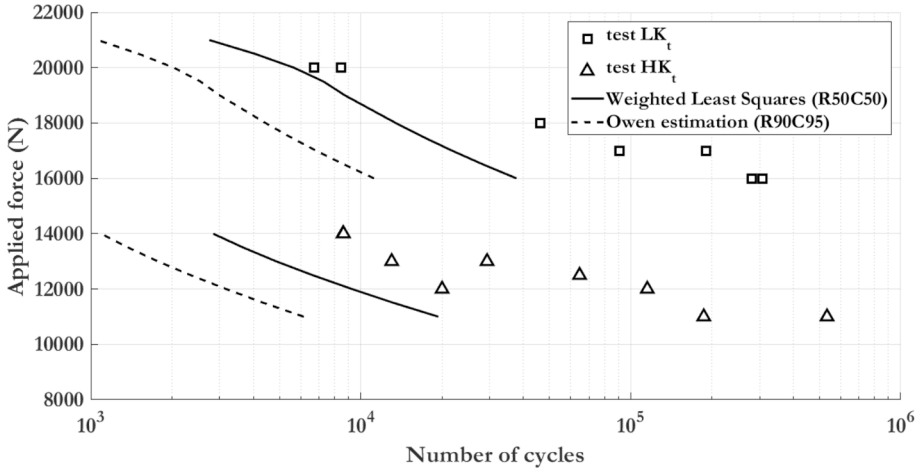

Fig. 11. Prediction of lifetime using the standard models identified in 3.3.1; Basquin's model with Weighted Least Squares method (black lines) and the statistically conservative fatigue model estimated with Owen method (black dotted lines).

$$\mathbf{R99C95}(\boldsymbol{ln}(\mathbf{N})) = \frac{(-\boldsymbol{ln}(0.99))^{\frac{1}{\mathbf{m}^{95\%}}}}{\Gamma\left(1+\frac{1}{\mathbf{m}^{95\%}}\right)}\overline{\boldsymbol{ln}(\mathbf{N})} \tag{31}$$

An absolute estimate of the distribution characteristics requires the calculation of the scaling factor noted μ_{struct}. This calculation considers the heterogeneity of the loading as well as the pure volume effect. It should be noted that it essentially involves the calculation of the I-factor (Eq. (31), which can be done by simple numerical integration in post-processing.

In practice, a discrete formulation of equation (Eq. (31) will be adopted and the calculation will be performed on each Gaussian point (integration point) of the simulation mesh. In this case, the function f^i becomes:

$$\begin{cases} \mathbf{f}^{\mathbf{i}}(\boldsymbol{ln}(\boldsymbol{N})) = \dfrac{\mathbf{V}_{\mathbf{g}}^{\mathbf{i}}}{\mathbf{V}_{\mathbf{o}}}\left(\dfrac{\boldsymbol{ln}(\mathbf{N})}{\boldsymbol{\mu}(\sigma^{\mathbf{i}})}\right)^{\mathbf{m}} \\ \mathbf{V}_{\mathbf{g}}^{\mathbf{i}} = \dfrac{\mathbf{V}_{\mathbf{e}}^{\mathbf{i}}}{\mathbf{Numberofgausspointsintheelement}} \end{cases} \tag{32}$$

The volume assigned to each Gauss point is the same for a given element. This formulation ensures that the possible stress gradient in an element is considered.

To determine the number of cycles for a given probability, the discrete version of equation Eq. (31) can be inverted, considering equation Eq. (33). This gives:

$$\begin{cases} P(\mathbf{ln}(\mathbf{N})) = 1 - \mathbf{exp}\left(-\dfrac{1}{\mathbf{V}_0}\sum_{\mathbf{i}=1}^{\mathbf{n_e}}\mathbf{V}_{\mathbf{g}}^{\mathbf{i}}\left(\dfrac{\mathbf{ln}(\mathbf{N})}{\frac{1}{\beta}\mathbf{ln}\left(\frac{\mathbf{c}}{\sigma^{\mathbf{i}}}\right)}\right)^{\mathbf{m}}\right) \\ N = \mathbf{exp}\left(\left(-\dfrac{\mathbf{ln}(1-\mathbf{P}(\mathbf{ln}(\mathbf{N})))}{\sum_{\mathbf{i}=1}^{\mathbf{n_e}}\frac{\mathbf{V}_{\mathbf{g}}^{\mathbf{i}}}{\mathbf{V}_0}\left(\frac{1}{\boldsymbol{\mu}(\sigma^{\mathbf{i}})}\right)^{\mathbf{m}}}\right)^{\frac{1}{\mathbf{m}}}\right) \end{cases} \tag{33}$$

4. Fatigue life assessment on notch specimens

All the previous approaches identified on smooth specimens were applied to the notch specimens introduced in 2.2. In the following, figures show the applied force as a function of the number of cycles to failure. The experimental results are represented by empty squares for LK_t specimens and empty triangles for HK_t specimens.

4.1. Standard approaches

The standard approaches detailed in 3.3.1 and 3.3.2 have been applied to estimate the lifetime of notched specimens. The regression model of Basquin identified with Weigthed Least Squares (R50C50) and the Owen model (R90C95) have been used to obtain

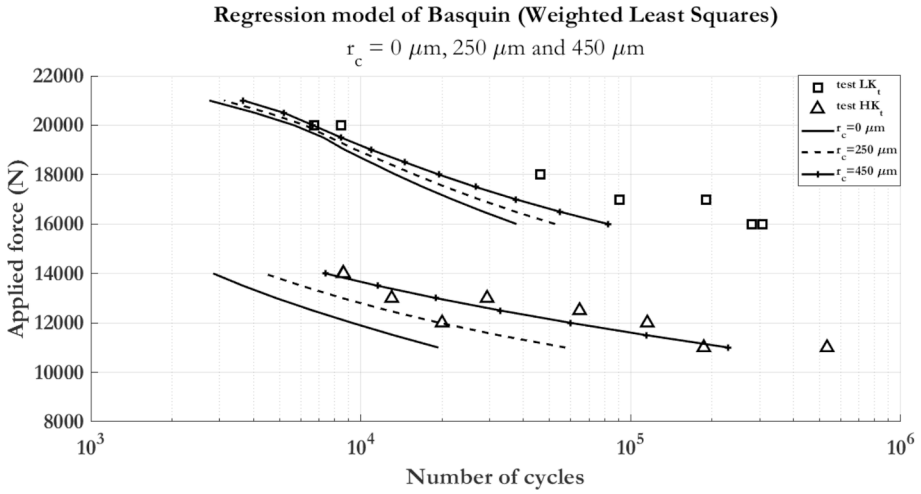

Fig. 12. Prediction of lifetime using the standard model identified in 3.3.1; regression of Basquin's model with Weighted Least Squares method considering stress gradient effect (r_c = 0, 250 and 450 μm).

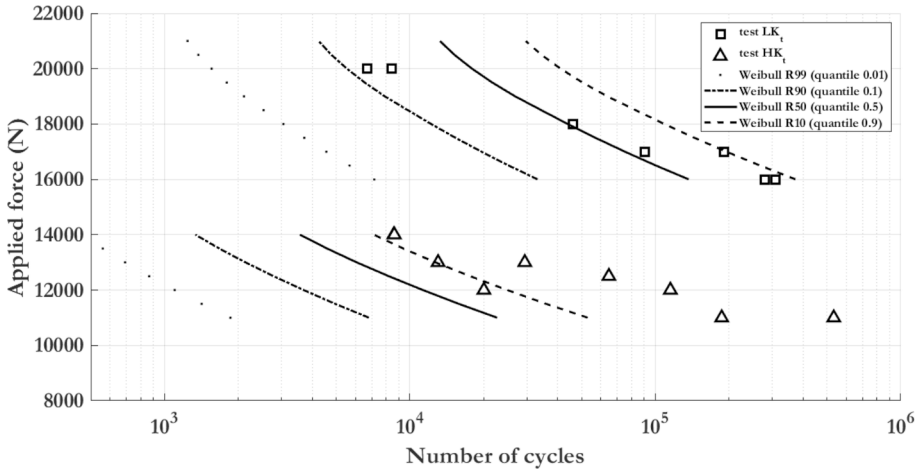

Fig. 13. Likely estimates of structural response with the fully probabilistic approach applied on the surface.

a mean and conservative estimate respectively. In addition, two assessments have been made, depending on whether the stress gradient effect is considered. The results are presented respectively in 4.1.1 and 4.1.2 sections.

4.1.1. Without stress gradient effect

The Fig. 11 compares the standard approach estimates with the experimental data. Both models lead to a lower lifetime prediction than that obtained experimentally. As expected, the Owen model is more conservative. This shows that even when a statistically conservative fatigue law is used, the standard approach is not sufficient as a component does not necessarily fail at its most loaded point. In fact, even if the macroscopic crack occurs in the area where the load is at its maximum, the stress gradient will inevitably affect microcrack propagation in the early stages of the fatigue damage. In what follows, it is then proposed to account for the effect of the stress gradient.

4.1.2. With stress gradient effect

The FCV method detailed in 3.3.2 to consider stress gradient effects has been applied here considering the two identified characteristic radii 250 μm and 450 μm. Predictions obtained with the different radii (dotted line for 250 μm and marked line for 450 μm) combined with the mean estimation (R50C50) are reported in Fig. 12 and compared to the experimental data. Predictions without taking account stress gradient effect are also plotted with solid lines. Note that the Owen conservative estimate (R90C95) is not shown, to improve the readability of the results. Similar trends were obtained with a greater degree of conservatism compared to the mean estimate (R50C50). From this figure, several results can be commented on. For a given specimen geometry, the higher the applied load, the lower the effect of the critical radius. This is related to plastification phenomena close to the notch. An increase in loading leads to

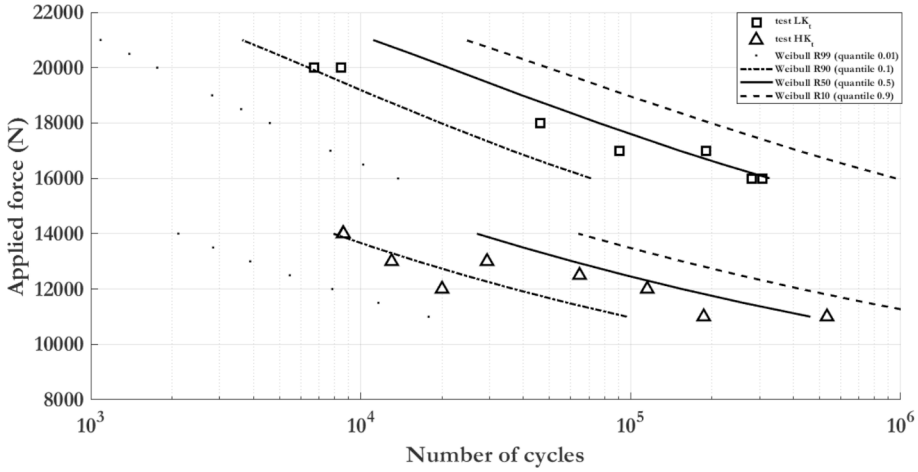

Fig. 14. Likely estimates of structural response with the fully probabilistic approach applied on the volume.

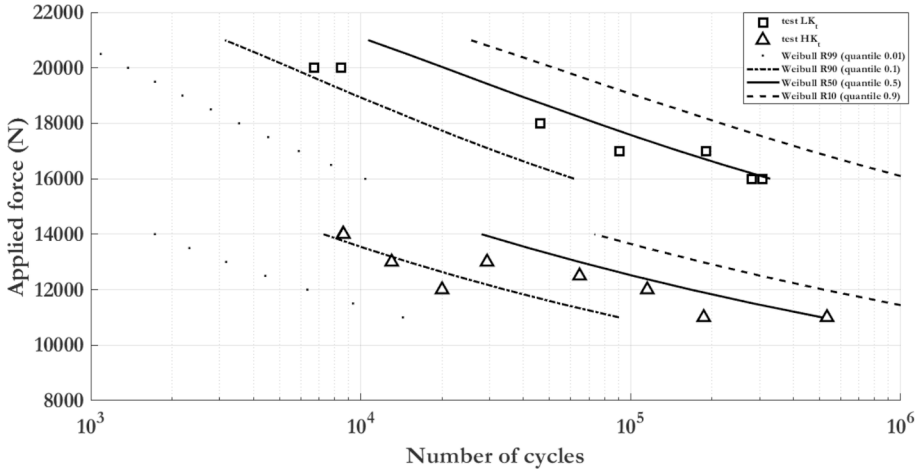

Fig. 15. Estimates of quantiles of structural response using conservatism with the fully probabilistic approach applied on the volume.

greater plastification at the bottom of the notch, which in turn reduces the stress gradient at depth. Thus, the use of FCV methodology has less impact at higher loads.

Moreover, the influence of the characteristic radius is more pronounced when the stress concentration K_t is increased. Fig. 7 shows that the effective stress gradient obtained at the lowest K_t is low. It was therefore expected that taking the gradient into account for this specimen geometry would have little effect on the fatigue life assessment. This is indeed the case here, where the estimated service life taking into account the gradient effect with the FCV method is too conservative for the lowest K_t, regardless of the characteristic radius considered. For the highest K_t, satisfying results are obtained by considering a characteristic radius $r_c = 450$ µm. This value appears to be higher than previously obtained in the literature with other approaches [55,56]. The fact that the methodology is not applicable for different K_t shows that it is not sufficiently effective. It therefore seems essential to consider scale effects.

4.2. *Probabilistic approaches*

To account for scale effects, it was decided to use a fully probabilistic “weakest link” approach. This involves closely coupling the probabilistic fatigue law of the volume element with the consideration of scale effects and stress heterogeneity. In other words, at each Gauss point of the structure, we consider the lifetime distribution as a function of stress. It is therefore no longer a matter of considering only the most critical point, as is the case with the standard approach presented above. Crack initiation on specimens with stress concentration generally occurs at the surface. In addition, the identification of the accelerated log Weibull model was carried out on smooth specimens, where crack initiation occurs mainly at the surface. Therefore, we first applied the surface formulation of the accelerated log Weibull law (Eq. (27) to the test data using the distribution identified in Table 2 in Section 3.4.1 (without conservatism only). Fig. 13 shows the experimental results for the two notched specimens and the lifetime estimates with different reliabilities (quantiles 0.5; 0.1; 0.01 and 0.9). Successful fatigue life assessment depends on the K_t considered. For the lowest K_t, the surface

probabilistic approach agrees well with the experimental data. For the highest K_t, however, the surface model appears to be too conservative. Again, these results must be considered in the light of the stress gradient induced by the two notches. In the case of the lowest K_t, the scaling effect will have the greatest effect on the results as the gradient effect is weak (Fig. 7). On the other hand, for the highest K_t, both the scale and the gradient effects should be considered. By using a surface probabilistic approach, the gradient effect is not properly considered as it is. A methodology combining the FCV method and the probabilistic surface approach could be considered. However, it would require the identification of a characteristic length, which is not readily available, as noted in the previous sections. Therefore, it was not investigated here, and a volume probabilistic approach was preferred to account for scale and gradient effects.

The fully probabilistic approach has been applied on the volume of the specimens. The two distributions identified in Table 2 Section 3.4.1 (without and with conservatism) have been used and the results are presented, respectively in Fig. 14 and Fig. 15. The impact of the two identified distributions is relatively low. This was expected in view of the small differences in values obtained for the various parameters. Finally, the modelling agrees with the experimental data for both specimen geometries, although the model has a slight tendency to overestimate the fatigue life of HK_t specimens. The choice of the classical Basquin hypothesis for both the LCF and HCF domains as illustrated in Fig. 10 could explain this trend. Thus, the volume approach correctly addresses the need to account for gradient effects and scale effects for Inconel 718 tested at 550 °C.

5. Conclusion

The objective of this paper was to implement and compare different fatigue post-processing approaches for fatigue life assessment of complex components, using Inconel 718 as an example. Tests at 550 °C on various specimen geometries highlighted factors such as mean stress, stress gradient, and scale effects. An elasto-visco-plastic behavior law was used for structural calculations, and the mechanical fields at stabilized cycle were analyzed for fatigue life assessment. Mean stress influence was incorporated through an effective stress in the fatigue model. Gradient and scaling effects were discussed with four post-processing approaches: Basquin's model with Weighted Least Squares, Owen's statistically conservative model, FCV method combined with standard approaches, and probabilistic approaches for scale effects.

The statistical approach, while accounting for scatter, was insufficient for stress concentrations. The FCV method showed promise but was limited by unaddressed scaling effects. Probabilistic surface and volume approaches were evaluated, with the volume approach proving effective for considering both scale and gradient effects without additional parameters.

Future work involves exploring non-parametric models like Gaussian processes to assess stress impact on lifetime variability, integrating physical and non-parametric models for better local variation identification.

CRediT authorship contribution statement

J.P. Goulmy: Writing – original draft, Investigation. **M. Kaminski:** Writing – original draft, Investigation, Data curation. **F.H. Leroy:** Writing – original draft, Supervision. **P. Kanoute:** Writing – original draft, Supervision, Investigation, Data curation, Conceptualization.

Declaration of competing interest

The authors declare that they have no known competing financial interests or personal relationships that could have appeared to influence the work reported in this paper.

Acknowledgement

The probabilistic development work has been largely supported by internal funding from Onera. The experimental data were obtained with the assistance of the French Technological Research Institute for Materials, Metallurgy and Processes (IRT M2P) under the CONDOR project. The authors would like to express their gratitude to IRT M2P and all the partners of the project led by IRT M2P. Safran is also acknowledged for its invaluable collaboration in this project.

Appendix A. . Identification method

This appendix describes the maximum likelihood (ML) identification method. The likelihood is the product of the values of the assumed probability density (Weibull) at the acquired measurement points. For the lifetime measurement (i) denoted $y^{(i)} = logN^{(i)}$, corresponding to loading $\sigma_{aeff}^{(i)}$ and therefore to a scaling factor $\mu^{(i)}$, this density is written:

$$f_Y\left(y^{(i)};\mu^{(i)},m\right) = \frac{m}{\mu^{(i)}}\left(\frac{y^{(i)}}{\mu^{(i)}}\right)^{m-1} exp\left\{-\left(\frac{y^{(i)}}{\mu^{(i)}}\right)^{m}\right\} \tag{A1}$$

The likelihood logarithm, L, can be deduced from this:

$$\begin{cases} L(C,\beta,m) = -\sum_{i=1}^{k} \boldsymbol{logy}^{(i)} + \sum_{i=1}^{k} \boldsymbol{logz}^{(i)} - \sum_{i=1}^{k} \boldsymbol{z}^{(i)} \\ \boldsymbol{y}^{(i)} = \boldsymbol{logN}^{(i)}, \quad \boldsymbol{z}^{(i)} = \left(\dfrac{\boldsymbol{y}^{(i)}}{\boldsymbol{\mu}^{(i)}}\right)^{\boldsymbol{m}}, \quad \boldsymbol{\mu}^{(i)} = \dfrac{1}{\boldsymbol{\beta}} \left(\boldsymbol{logC} - \boldsymbol{log\sigma}_{\boldsymbol{aeff}}^{(i)}\right) \end{cases} \tag{A2}$$

L is maximized numerically, taking the optimal parameters as retained estimates. Optimization can be performed most efficiently using Fisher's scoring algorithm [57], also known as Iteratively Reweighted Least Squares. This is a Newton-Raphson type approach in which the Hessian is replaced by its mean value [58]. The opposite of this mean value is called the Fisher K information matrix. The components of the Jacobian are called U-score functions. Noting generically θ the vector of parameters to be optimized, its iterative update from an initial estimate is performed as follows at step $j + 1$:

$$\boldsymbol{\theta}^{j+1} = \boldsymbol{\theta}^{j} + \boldsymbol{inv}(\boldsymbol{K}_{\boldsymbol{\theta\theta}}) \cdot \boldsymbol{U}_{\boldsymbol{\theta}} \tag{A3}$$

Let's now consider our special case and introduce various matrix notations.

$$\begin{cases} \theta = \left(P^T, m\right)^T \text{ vector of parameters to be identified} \\ \qquad\qquad\qquad\qquad (logC)^T \end{cases}$$

$$\begin{cases} \mu = \left(\mu^{(1)}, \cdots, \mu^{(i)}, \cdots, \mu^{(k)}\right)^T \\ X \text{ tq } X_{i,1} = log\sigma_{aeff}^{(i)} \text{ et } X_{i,2} = 1 \end{cases} \quad \Rightarrow \quad \mu = X \cdot P$$

$$\begin{cases} z = \left(z^{(1)}, \cdots, z^{(i)}, \cdots, z^{(k)}\right)^T \text{ with } z^{(i)} = \left(logN^{(i)} / \mu^{(i)}\right)^m \\ s = \left(z^{(1)} - 1, \cdots, z^{(i)} - 1, \cdots, z^{(k)} - 1\right)^T \end{cases}$$

$$\begin{cases} W \text{ tq } \boldsymbol{W}_{i,i} = \left(1/\boldsymbol{\mu}^{(i)}\right)^2 \text{ et } \boldsymbol{W}_{i,j\neq i} = 0 \\ \widetilde{\boldsymbol{W}} \text{ tq } \widetilde{\boldsymbol{W}}_{i,i} = \left(1/\boldsymbol{\mu}^{(i)}\right)^2 \left(1 - (1+\boldsymbol{m})\boldsymbol{z}^{(i)}\right) \text{ et } \widetilde{\boldsymbol{W}}_{i,j\neq i} = 0 \end{cases} \tag{A4}$$

Optimization of the Basquin distribution parameters P and the Weibull modulus m can be carried out in a decoupled way if the initial estimate is of satisfactory quality (close to optimal):

$$\begin{cases} \boldsymbol{P}^{j+1} = \boldsymbol{P}^{j} + inv(\boldsymbol{K}_{\boldsymbol{PP}}) \cdot \boldsymbol{U}_{\boldsymbol{P}} \\ \boldsymbol{m}^{j+1} = \boldsymbol{m}^{j} + inv(\boldsymbol{K}_{\boldsymbol{mm}}) \cdot \boldsymbol{U}_{\boldsymbol{m}} \end{cases} \tag{A5}$$

The scores and corresponding information matrices are then detailed below:

$$\begin{cases} \boldsymbol{U}_{\boldsymbol{P}} = m\, \boldsymbol{X}^T \boldsymbol{W}^{1/2} s \\ \boldsymbol{U}_{\boldsymbol{m}} = \dfrac{\boldsymbol{k}}{\boldsymbol{m}} - \dfrac{1}{\boldsymbol{m}} \sum_{i=1}^{k} \left(\boldsymbol{z}^{(i)} - 1\right) \boldsymbol{logz}^{(i)} \\ \boldsymbol{K}_{\boldsymbol{PP}} = -m\, \boldsymbol{X}^T \widetilde{\boldsymbol{W}} X \\ \boldsymbol{K}_{\boldsymbol{mm}} = \dfrac{\boldsymbol{k}}{\boldsymbol{m}^2} + \dfrac{1}{\boldsymbol{m}^2} \sum_{i=1}^{k} \boldsymbol{z}^{(i)} \left(\boldsymbol{logz}^{(i)}\right)^2 \end{cases} \tag{A6}$$

The entire procedure has been implemented in Matlab. Note that it is technically more robust to treat Eq. (A.5) as a least-squares solution (function \ in Matlab) than to invert the K matrices. For example, we solve systems $\boldsymbol{K}_{PP}\Delta P = U_P$ with $\Delta P = P^{j+1} - P^{j}$. Finally, an optimal estimate of m and $P = (-1/\beta,\ 1/\beta \cdot logC)^T$ is obtained and β and C, parameters of the Basquin distribution are identified.

The estimate of the modulus m is classically biased when identifying a "simple" one-dimensional Weibull distribution. A limited number of measurements (<50) leads to a significant overestimation of m. Tabulated correction coefficients are available for this [59]. This bias also exists in our context of Weibullian log-life regression, but analytical corrections are less readily available [54]. We have chosen to estimate the bias using the boostrap technique [60], which simultaneously allows to estimate the identification uncertainty (see Appendix B).

Appendix B. . Uncertainty, conservatism and confidence identification

Imposing a confidence of 95 %, which we note R99C95, means that we want an estimate of R99 that has a 95 % chance of being lower than its real value. This is called the tolerance bound, which some also note $K_{0.99,0.95,k}$ where k is the number of measurements processed. This notation serves as a reminder that the uncertainty and therefore the allowance depends on k. Considering the notion of confidence presupposes knowledge of the distribution of the uncertainty of estimation of the target quantile/percentile. This is shown as a dotted line around the P percentile on the Fig. B.1. This distribution is well known if we consider the one-dimensional Weibull distribution of log N at imposed loading $log\sigma_{aeff}$ [61]. The reduction factor can then be estimated as follows:

$$\begin{aligned}
\mathbf{K}_{1-\mathbf{p},\mathbf{C},\mathbf{n}} &= \widehat{\mathbf{Q}}(p)\cdot\gamma(m,k,p,C)\\
\gamma(m,k,p,C) &= \mathbf{e}^{-\frac{\mathbf{V}(\mathbf{k},\mathbf{p},\mathbf{C})}{\mathbf{m}\sqrt{\mathbf{k}}}} \le 1\\
V(k\ge 16,\ 0.1,\ 95\%) &\approx 3.803 + \mathbf{exp}\left\{1.79 - 0.516\ \mathbf{log}(\mathbf{k}) + \frac{5.1}{\mathbf{k}-1}\right\}\\
V(k\ge 16,\ 0.01,\ 95\%) &\approx 6.649 + \mathbf{exp}\left\{2.55 - 0.526\ \mathbf{log}(\mathbf{k}) + \frac{4.76}{\mathbf{k}}\right\}
\end{aligned} \tag{B1}$$

Tabulated values of $V(k,p,95\%)$ are also available in [61] for a number of measurements k < 16 and p = 0.1 or 0.01 (admissible values B and A). It should be noted that the m value is to be used here without debiasing.

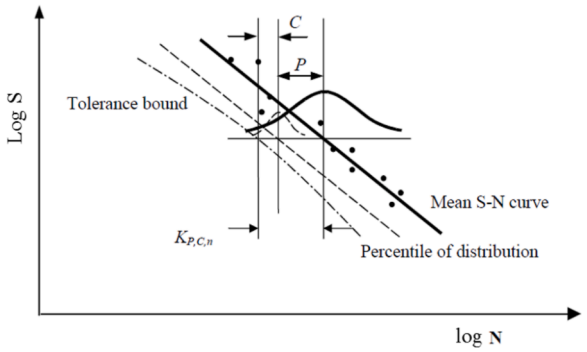

Fig. B1. Lowering the estimate of a percentile P to obtain a confidence C for a lognormal distribution ([62]).

However, the identification of a tolerance limit is based on two-dimensional service life data $logN - log\sigma_{aeff}$ and requires the identification of model parameters (C,β,m). This identification by regression is itself uncertain, and an additional allowance must therefore be made. We know that the prediction of a regression is more uncertain the closer you are to one end of the identification domain [63]. A tolerance limit should therefore be concave, with abatements greater than the extremes, as suggested by the Eq. (B.1). Estimates are classically available for a lognormal distribution [62], as this corresponds to linear regression with Gaussian noise in a log–log plot. However, to the best of our knowledge, there are no classically used estimates for an accelerated log-Weibull distribution.

The bootstrap technique [60] makes it possible to efficiently quantify the uncertainty distribution associated with any estimator, in this case a quantile, when this distribution is not easy to formulate from a theoretical point of view. The method consists in re-sampling the measurements with a discount by reproducing the estimation procedure, this step being iterated a large number of times. The result is a large number of estimates of the target quantile, constituting a sample of the identification uncertainty. We then select the 5th empirical percentile to obtain the 95 % confidence estimate. As an example, we obtain R99C95 by carrying out 10,000 bootstraps (resampling) with as many estimates of R99 (quantile 0.01). The 500th lowest estimate (5th percentile) corresponds to R99C95 with fairly good precision. Note that when the number of measurements is low, the diversity obtained by resampling is limited. To extend it, it is preferable to randomly draw new lifetime samples (in identical numbers) from the probabilistic lifetime model identified. This approach is called smoothed bootstrap. As an illustration, we have applied it in Fig. B.2 to a synthetic example with a reduced number of measurements.

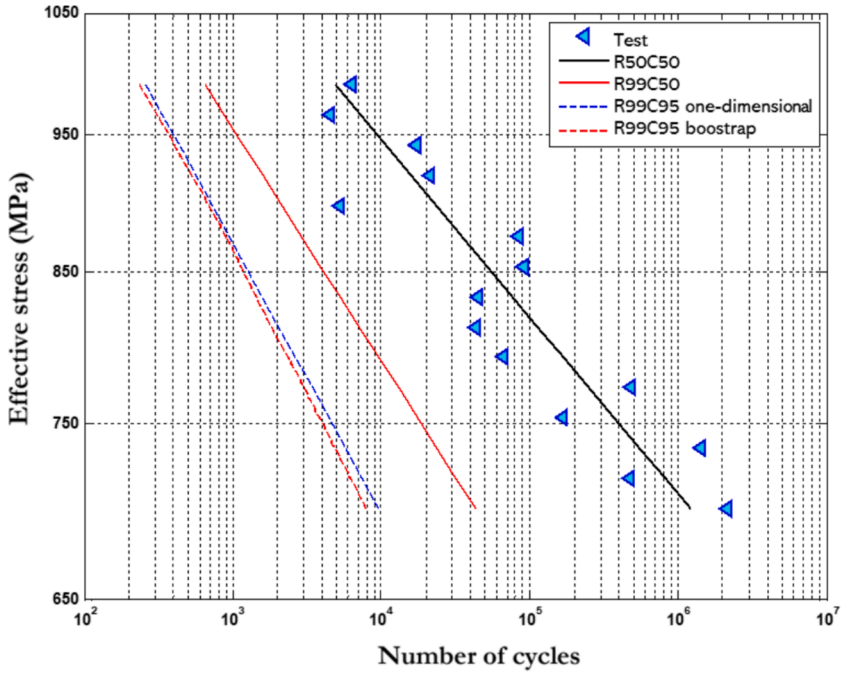

Fig. B2. Artificial example of R99 adjustment (R99C50) and R99C95 bootstrap correction giving 95 % confidence (10,000 bootstraps). Also shown is the one-dimensional correction proposed in Eq. .

It can be seen that the introduction of 95 % confidence lowers the standard estimate of R99 (R99C50), but does not show a marked non-linear trend. The bootstrapped tolerance limit is almost identical to the one-dimensional correction proposed in Eq. B(1), which is linear. We attribute this to the fact that the Weibull distribution has a strong tail and therefore "assimilates" measurements far from the mean value more easily than a Gaussian distribution. In other words, the presence of extreme points has less impact on the estimation of mean behavior. Measurements located at the extremes of the domain do not have a particularly high leverage on maximum likelihood. This would explain why the tolerance limit at the extremes (concavity) is not significantly further from the mean value. Increasing the number of measurements beyond the fifteen taken as an example would weaken the already negligible non-linearity. In the end, we retain the linear approximations of the tolerance limits obtained by bootstrap. The parameters of these log–log scale regressions are equated $P = (-1/\beta,\ 1/\beta \cdot logC)^T$ to obtain the Basquin parameters β and C of each tolerance limit (for example β^{R99C95} and C^{R99C95}).

$$\begin{cases} \widehat{\boldsymbol{m}}^{95\%} = \dfrac{\boldsymbol{log}[\boldsymbol{log}(0.99)/\boldsymbol{log}(0.9)]}{\boldsymbol{log}\left[\overline{\boldsymbol{R99C95}(\sigma_{aeff})/\boldsymbol{R90C95}(\sigma_{aeff})}\right]} = \dfrac{-2.3497819}{\boldsymbol{log}\left[\overline{\boldsymbol{R99C95}(\sigma_{aeff})/\boldsymbol{R90C95}(\sigma_{aeff})}\right]} \\ \boldsymbol{\mu}^{95\%} = R99C95(\sigma_{aeff}) \cdot [\boldsymbol{log}(1/0.99)]^{-1/\widehat{\boldsymbol{m}}^{95\%}} \end{cases}$$

$$= \frac{1}{\boldsymbol{\beta}^{R99C95}}\ \boldsymbol{log}\left(\frac{\boldsymbol{C}^{R99C95}}{\sigma_{aeff}}\right) \cdot 0.010050336^{-1/\widehat{\boldsymbol{m}}^{95\%}} \tag{B2}$$

where the mean value $\overline{R99C95(\sigma_{aeff})/R90C95(\sigma_{aeff})}$ is a constant independent of σ_{aeff} which approximates this ratio with very good accuracy. We can also define Basquin parameters corresponding to $\mu^{95\%}$:

$$\begin{cases} \boldsymbol{\beta}^{95\%} = \boldsymbol{\beta}^{R99C95} \Big/ 0.010050336^{-1/\widehat{\boldsymbol{m}}^{95\%}} \\ \boldsymbol{C}^{95\%} = \boldsymbol{C}^{R99C95} \end{cases} \tag{B3}$$

This downgraded identification corresponds to a deliberate overestimation of the dispersion $\widehat{m}^{95\%} < \widehat{m}$ and a slight decrease in the characteristic lifetime $\mu^{95\%} < \mu$. This is illustrated in the paper on real lifetime data.

Data availability

The data that has been used is confidential.

References

[1] Chaboche JL, Kanouté P, Azzouz F. Cyclic inelastic constitutive equations and their impact on the fatigue life predictions. Int J Plast 2012;35:44–66. https://doi.org/10.1016/j.ijplas.2012.01.010.
[2] Kamaya M, Kawakubo M. Mean stress effect on fatigue strength of stainless steel. Int J Fatigue 2015;74:20–9. https://doi.org/10.1016/j.ijfatigue.2014.12.006.
[3] Zhu S-P, Ye W-L, Correia JAFO, Jesus AMP, Wang Q. Stress gradient effect in metal fatigue: review and solutions. Theor Appl Fracture Mech 2022;121. https://doi.org/10.1016/j.tafmec.2022.103513.
[4] Härkegård G, Halleraker G. Assessment of methods for prediction of notch and size effects at the fatigue limit based on test data by Böhm and Magin. Int J Fatigue 2010;32(10):1701–9. https://doi.org/10.1016/j.ijfatigue.2010.03.011.
[5] He J-C, Zhu S-P, Luo C, Niu X, Wang Q. Size effect in fatigue modelling of defective materials: Application of the calibrated weakest-link theory. Int J Fatigue 2022;165. https://doi.org/10.1016/j.ijfatigue.2022.107213.
[6] Chen Q, Kawagoishi N, Nisitani H. Evaluation of notched fatigue strength at elevated temperature by linear notch mechanics. Int J Fatigue 1999;21(9):925–31. https://doi.org/10.1016/S0142-1123(99)00081-X.
[7] Amargier R, Fouvry S, Chambon L, Schwob C, Poupon C. Stress gradient effect on crack initiation in fretting using a multiaxial fatigue framework. Int J Fatigue 2010;32(12):1904–12. https://doi.org/10.1016/j.ijfatigue.2010.06.004.
[8] Alexandre F, Deyber S, Pineau A. Modelling the optimum grain size on the low cycle fatigue life of a Ni based superalloy in the presence of two possible crack initiation sites. Scripta Materialia 2004;50(1):25–30. https://doi.org/10.1016/j.scriptamat.2003.09.043.
[9] Maderbacher H, Oberwinkler B, Gänser H-P, Tan W, Rollett M, Stoschka M. The influence of microstructure and operating temperature on the fatigue endurance of hot forged Inconel® 718 components. Mater Sci Eng: A 2013;585:123–31. https://doi.org/10.1016/j.msea.2013.07.053.
[10] Gallerneau F. « Etude et modélisation de l'endommagement d'un superalliage monocristallin revêtu pour aube de turbine », Text, Ecole des Mines de Paris, 1995.
[11] Lemaitre J, J.-L. Chaboche, A. Benallal, et R. Desmorat, Mécanique des matériaux solides - 3ème édition, 3e édition. Paris: Dunod, 2009.
[12] Lemaitre J, R. Desmorat, et M. Sauzay, Loi d'évolution de l'endommagement anisotrope, Comptes Rendus de l'Académie des Sciences - Series IIB - Mechanics-Physics-Astronomy, vol. 327, no 12, p. 1231-1236, nov. 1999, doi: 10.1016/S1287-4620(00)88646-9.
[13] Kaminski M, Modélisation de l'endommagement en fatigue des superalliages monocristallins pour aubes de turbines en zone de concentration de contrainte, phdthesis, École Nationale Supérieure des Mines de Paris, 2007.
[14] Smith KN, Topper TH, Watson P. A Stress-strain Function for the Fatigue of Metals Defense Technical. Information Center; 1969.
[15] Crossland B. Effect of large hydrostatic pressures on the torsional fatigue strength of an alloy steel Londres Institution of Mechanical Engineers 1956.
[16] Sines G, Ohgi G. Fatigue criteria under combined stresses or strains. J Eng Mater Technol 1981;103(2):82–90. https://doi.org/10.1115/1.3224995.
[17] Gonçalves CA, Araújo JA, Mamiya EN. Multiaxial fatigue: a stress based criterion for hard metals. Int J Fatigue 2005;27(2):177–87. https://doi.org/10.1016/j.ijfatigue.2004.05.006.
[18] Palin-Luc T, Lasserre S. An energy based criterion for high cycle multiaxial fatigue. Eur J Mech - A/Solids 1998;17(2):237–51. https://doi.org/10.1016/S0997-7538(98)80084-3.
[19] Brown MW, Miller KJ. A theory for fatigue failure under multiaxial stress-strain conditions. Proc Instit Mech Eng 1973;187(1):745–55. https://doi.org/10.1243/PIME_PROC_1973_187_069_02.
[20] Fatemi A, Socie DF. A critical plane approach to multiaxial fatigue damage including out-of-phase loading, Fatigue & Fracture of Engineering Materials & Structures, vol. 11, no 3, p. 149-165, mars 1988, doi: 10.1111/j.1460-2695.1988.tb01169.x.
[21] Robert J-L. Contribution à l'étude de la fatigue multi axiale sous sollicitations periodiques ou aléatoires. INSA: Lyon; 1992.
[22] Bonnand V, Chaboche JL, Gomez P, Kanouté P, Pacou D. Investigation of multiaxial fatigue in the context of turboengine disc applications. Int J Fatigue 2011;33(8):1006–16. https://doi.org/10.1016/j.ijfatigue.2010.12.018.
[23] Peterson RE. The role of stress distribution in fatigue, Experimental Mechanics, vol. 1, no 4, p. 105-115, avr. 1961, doi: 10.1007/BF02323115.
[24] Neuber H. Theory of notch stresses: principles for exact calculation of strength with reference to structural form and material; 1961.
[25] Li C, Xie LY, Xie YJ, Liu SL, Mu T, Xu XY. Calculation of characteristic size and fatigue life of structural members with blunt notches. Eng Fracture Mech 2020;239. https://doi.org/10.1016/j.engfracmech.2020.107310.
[26] Hild F, Marquis D. A statistical approach to the rupture of brittle materials. Eur J Mech Solids 1992;11:753–65.
[27] Delahay T, Palin-Luc T. Estimation of the fatigue strength distribution in high-cycle multiaxial fatigue taking into account the stress–strain gradient effect. Int J Fatigue 2006;28(5):474–84. https://doi.org/10.1016/j.ijfatigue.2005.06.048.
[28] Karlén K, Olsson M. A probabilistic model for the entire HCF domain based on equivalent stress – simulations and experiments. Int J Fatigue 2012;36(1):9–17. https://doi.org/10.1016/j.ijfatigue.2011.09.007.
[29] Weibull W. A statistical theory of the strength of materials. Generalstabens litografiska anstalts förlag 1939.
[30] Weibull W. A statistical distribution function of wide applicability. J Appl Mech 1951:293–7.
[31] Karolczuk A, Palin-Luc T. Modelling of stress gradient effect on fatigue life using Weibull based distribution function. J Theor Appl Mech 2013;51(2):297–311.
[32] Alexandre F. Aspects probabilistes et microstructuraux de l'amorçage des fissures de fatigue dans l'alliage Inco 718. Ecole des mines de Paris, Paris: Thèse de doctorat; 2004.
[33] Maderbacher H, T. Christiner, H.-P. Gänser, M. Riedler, M. Stoschka, et W. Eichlseder, Lifetime evaluation of hot forged aerospace components by linking microstructural evolution and fatigue behaviour, Procedia Eng, 2 (1), 2269-2276, 2010, doi: 10.1016/j.proeng.2010.03.243.
[34] Goulmy JP, et al., A calibration procedure for the assessment of work hardening part I: Effects of the microstructure and load type, Mater Characteriz, 175, 111067, 2021, doi: 10.1016/j.matchar.2021.111067.
[35] Muhammad M, Frye P, J. Simsiriwong, S. Shao, et N. Shamsaei, An investigation into the effects of cyclic strain rate on the high cycle and very high cycle fatigue behaviors of wrought and additively manufactured Inconel 718, Int J Fatigue, 144, 106038, 2021, doi: 10.1016/j.ijfatigue.2020.106038.
[36] Connoley T, Reed PAS, Starink JM. Short crack initiation and growth at 600°C in notched specimens of Inconel 718. Mater Sci Eng 2003;340:139–54.
[37] Goulmy JP et al., A calibration procedure for the assessment of work hardening Part II: Application to shot peened IN718 parts, Mater Charact, vol. 175, p. 111068, mai 2021, doi: 10.1016/j.matchar.2021.111068.
[38] Kruch S, Kanoute P, Bonnand V. Oneras multiaxial and anisothermal lifetime assessment for engine components, AerospaceLab J, (9), p. 12 pages, 2015, doi: 10.12762/2015.AL09-08.
[39] Lee Y-L, Taylor D. Fatigue Testing and Analysis: Theory and Practice. Butterworth-Heinemann; 2005.
[40] Morel F, Palin-Luc T. A non-local theory applied to High-cycle multiaxial fatigue. Fatigue Fracture Eng Mater Struct 2002;25:649–65. https://doi.org/10.1046/j.1460-2695.2002.00527.x.
[41] Banvillet A, Palin-Luc T, Lasserre S. A volumetric energy based high cycle multiaxial fatigue citerion, Int J Fatigue, vol. 25, no 8, p. 755-769, 2003, doi: 10.1016/S0142-1123(03)00048-3.
[42] Morel F, Flacelière L. Data scatter in multiaxial fatigue: from the infinite to the finite fatigue life regime, Int J Fatigue, 27 (9), p. 1089-1101, sept. 2005, doi: 10.1016/j.ijfatigue.2005.01.009.
[43] Z-set – Non-linear material and structure analysis suite. http://zset-software.com/.
[44] Bathias C, Pineau A. Fatigue of Materials and Structures: Application to Design and Damage | Wiley.

[45] ASTM E739, « Practice for Statistical Analysis of Linear or Linearized Stress-Life (S-N) and Strain-Life (E-N) Fatigue Data », ASTM International, 2015. doi: 10.1520/E0739-10R15.
[46] Sudret B ,Z. Guédé, « Probabilistic assessment of thermal fatigue in nuclear components », Nuclear Engineering and Design, vol. 235, no 17-19, p. 1819-1835, août 2005, doi: 10.1016/j.nucengdes.2005.05.016.
[47] Hochard C, Lahellec N, Bordreuil C., A ply scale non-local fibre rupture criterion for CFRP woven ply laminated structures, Composite Struct, 80 (3), p. 321-326, oct. 2007, doi: 10.1016/j.compstruct.2006.05.021.
[48] Thieulot-Laure E. Méthode probabiliste unifiée pour la prédiction du risque de rupture en fatigue, phdthesis, École normale supérieure de Cachan - ENS Cachan, 2008.
[49] Karlén K, Olsson M. A probabilistic model for the entire HCF domain based on equivalent stress – Simulations and experiments, Int J Fatigue, vol. 36, no 1, p. 9-17, mars 2012, doi: 10.1016/j.ijfatigue.2011.09.007.
[50] Schijve J. A normal distribution or a weibull distribution for fatigue lives. Fatigue Fract Engng Mater Struct 1993;16(8):851–9. https://doi.org/10.1111/j.1460-2695.1993.tb00124.x.
[51] Muniz-Calvente M, de Jesus AMP, Correia JAFO, et A. Fernández-Canteli, « A methodology for probabilistic prediction of fatigue crack initiation taking into account the scale effect », Engineering Fracture Mechanics, vol. 185, p. 101-113, nov. 2017, doi: 10.1016/j.engfracmech.2017.04.014.
[52] Lawless JF. Statistical models and methods for lifetime data. John Wiley & Sons; 2011.
[53] Hild F, Forquin P, Cordeiro da Silva AR. Single and multiple fragmentation of brittle geomaterials. Revue Française de Génie Civil 2003;7:973–2003.
[54] Prudente AA, Cordeiro GM. Generalized Weibull linear models, Communications in Statistics - Theory and Methods, vol. 39, no 20, p. 3739-3755, oct. 2010, doi: 10.1080/03610920903350580.
[55] Eriksson R, Simonsson K, Leidermark D, Moverare J. Evaluation of notch effects in low cycle fatigue of alloy 718 using critical distances. MATEC Web Conf, 2018;165:15001. https://doi.org/10.1051/matecconf/201816515001.
[56] Solberg K, Wan D, Berto F. Fatigue assessment of as-built and heat-treated Inconel 718 specimens produced by additive manufacturing including notch effects. Fatigue Fract Engng Mater Struct 2020;43(10):2326–36. https://doi.org/10.1111/ffe.13300.
[57] Fisher RA. Theory of Statistical Estimation, Mathematical Proceedings of the Cambridge Philosophical Society, vol. 22, no 5, p. 700-725, juill. 1925, doi: 10.1017/S0305004100009580.
[58] Jennrich RI, Sampson PF. Newton-Raphson and related algorithms for maximum likelihood variance component estimation. Technometrics 1976;18(1):11–7. https://doi.org/10.2307/1267911.
[59] « Standard Practice for Reporting Uniaxial Strength Data and Estimating Weibull Distribution Parameters for Advanced Ceramics.
[60] Efron B, Tibshirani RJ. An Introduction to the Bootstrap. New York: Chapman and Hall/CRC; 1994. 10.1201/9780429246593.
[61] United States Department of Defense, Military handbook - MIL-HDBK-17-1F. Volume 1, Polymer matrix composites guidelines for characterization of structural materials: composite materials handbook. Place of publication not identified: U.S. Department of Defense, 2002.
[62] Ronold KO, Echtermeyer AT. « Estimation of fatigue curves for design of composite laminates », Composites Part A: Applied Science and Manufacturing, vol. 27, no 6, p. 485-491, janv. 1996, doi: 10.1016/1359-835X(95)00068-D.
[63] Cornillon P-A, Matzner-Løber É. Régression: théorie et applications. in Statistiques et probabilités appliquées. Paris Berlin Heidelberg [etc.]: Springer; 2006.